TANDEM RNA AFFINITY PURIFICATIONS TO STUDY AN ESSENTIAL SNORNA IN RIBOSOME ASSEMBLY

DANIEL GIOVANNI ROCCA
Bachelor of Science, **University of Lethbridge, 2020**

A thesis submitted
in partial fulfilment of the requirements for the degree of

MASTER OF SCIENCE

in

BIOCHEMISTRY

Department of Chemistry and Biochemistry
University of Lethbridge
LETHBRIDGE, ALBERTA, CANADA

TANDEM RNA AFFINITY PURIFICATIONS TO STUDY AN ESSENTIAL SNORNA IN RIBOSOME ASSEMBLY

DANIEL GIOVANNI ROCCA

Date of Defence: December 15, 2022

Dr. U. Kothe	Professor	Ph.D.
Dr. M. Roussel	Professor	Ph.D.
Thesis Co-Supervisors		
Dr. H.J. Wieden	Professor	Ph.D.
Thesis Examination Committee Member		
Dr. S. Wetmore	Professor	Ph.D.
Thesis Examination Committee Member		
Dr. M. Dosil	Professor	Ph.D.
External Examiner		
Universidad de Salamanca		
Salamanca, Spain		
Dr. M. Gerken	Professor	Ph.D.
Chair, Thesis Examination Committee		

Dedication

To my late great aunt, Phyllis Jordan, who supported all my goals and aspirations, including writing this thesis.

Abstract

Eukaryotic ribosome assembly is an essential process involving many protein and RNA assembly factors. Mutations of genes encoding ribosomal proteins or assembly factors can result in diseases in humans. The upregulation of ribosome assembly is also a hallmark of many cancers. snR30 is an interesting assembly factor due to its role as an unusual and essential H/ACA small nucleolar RNA and as it is one of only three essential RNA assembly factors. Here, I have developed a system for the co-expression of aptamer-tagged variants of snR30 and truncations of ribosomal RNA in *Saccharomyces cerevisiae*. Next, I optimized the tandem purifications of the snR30-bound pre-ribosomes utilizing these aptamers. In conclusion, my system will allow for in-depth characterization of the composition and structure of snR30-bound ribosome precursors. This characterization will improve the understanding of the essential activity of snR30 for ribosome assembly in yeast and inform future studies on the function of the homologous U17 RNA in humans.

Acknowledgements

The work entailed in this thesis could not have been accomplished without the support and encouragement of a large group of people. I would like to thank the members of the Kothe lab, past and present, for their patience, advice, and feedback throughout the last two years. I would also like to thank Dr. Kothe for her support and assistance working within her lab and the many opportunities she has given me to develop further as a scientist during my degree. As well, many thanks to Dr. Roussel for joining my thesis committee as a co-supervisor. His perspective on this project and efforts as a liaison to the University of Lethbridge during my time working in Winnipeg have been of great help during this time. I would like to thank Dr. Wieden, and Dr. Wetmore for their suggestions and feedback as this project developed, as well as Dr. Dosil for agreeing to lend her insight into this project as an external examiner. Finally, I would like to thank Dr. Gerken for agreeing to act as chair for my thesis defence.

Table of Contents

List of Tables

List of Figures

List of Abbreviations

AMV	Avian myeloblastosis virus
bp	Base pair
Cryo-EM	Cryo-electron microscopy
DAmP	Decreased abundance by mRNA perturbation
DMSO	Dimethyl sulfoxide
dNTP	Deoxyribonucleotide triphosphate
EDTA	Ethylenediaminetetraacetic acid
ES6	Expansion segment 6
ETS	Externally transcribed spacer
H box	Hinge box
IPTG	Isopropyl β-d-1-thiogalactopyranoside
ITS	Internally transcribed spacer
LB	Lysogeny broth
LSU	Large subunit
MBP	Maltose binding protein
MWCO	Molecular weight cut-off
nt	Nucleotide
PAGE	Poly-acrylamide gel electrophoresis
PEG	Polyethylene glycol
pHMM	Plasmid for histidine MS2 maltose binding protein
PolI	Polymerase I
PolII	Polymerase II
rDNA	Ribosomal deoxyribonucleic acid
RNP	Ribonucleoprotein

r-proteins	Ribosomal proteins
rRNA	Ribosomal ribonucleic acid
RT-PCR	Reverse transcription polymerase chain reaction
SC	Synthetic complete
snoRNA	Small nucleolar ribonucleic acid
snR30	Small nucleolar RNA 30
SSU	Small subunit
TAP	Tandem affinity purification
Tob	Tobramycin
UTP	U3 Protein
YNB	Yeast nitrogen base
YPD	Yeast extract-peptone-dextrose
YPG	Yeast extract-peptone-galactose

Chapter 1: Introduction

1.1 Ribosomes are an essential component of cellular function

The ribosome is a complex biological machine that is essential for the growth and division of cells across all domains of life because the ribosome synthesizes all cellular proteins. A complex of ribosomal proteins (r-proteins) around a catalytic core of ribosomal RNAs (rRNAs) composes each of the two subunits of the mature ribosome, which must come together to facilitate the process of translation, by which all cellular proteins are made. The assembly of the ribosome is, therefore, an essential process for cells, and its dysregulation, e.g., through mutations, is a cause of a wide array of diseases in humans. Diseases resulting from mutations genes encoding ribosomal proteins or ribosome assembly are known as ribosomopathies. Ribosomopathies are directly linked to a dysfunction of ribosome production [1-6]. For example, Dyskeratosis congenita is a disease arising form mutations of genes encoding proteins that are part of H/ACA small nucleolar ribonucleoproteins and/or the telomerase complex, including dyskerin [7]. Additionally, the upregulation of ribosome production is linked to multiple forms of cancer. However, the treatment of these diseases and the broader understanding of the process of ribosome assembly is hindered by the complexity of the ribosome assembly pathway and the transient nature of many essential steps. While several steps of ribosomal synthesis have been identified as potential targets for the treatment of cancers [6, 8], further improvements to the understanding of ribosome assembly have the potential to open additional avenues for treating conditions that arise from the dysregulation of the function, and assembly of the ribosome [5, 7, 9].

In order to investigate ribosome biogenesis in detail, it is often necessary to utilize model organisms that can be studied with greater ease than human cells due to their growth rate, growth conditions, and ease of genetic manipulation. Despite differences in specific steps and

factors involved in the process of assembly across different eukaryotes, the process remains sufficiently similar, both in terms of the overall process and the presence of individual events, that important insight can be gleaned into the function of human cells using studies in other eukaryotes [10, 11]. Because of this, studies of ribosome assembly in model eukaryotes such as *Saccharomyces cerevisiae, Chaetomium thermophilum,* and *Schizosaccharomyces pombe* are often used to inform analysis of the homologous processes in human cells in addition to increasing our understanding of the cellular function of these organisms. In this thesis, I explore the assembly of ribosomes using baker's yeast *S. cerevisiae,* which functions as a typical model organism for the study of ribosome assembly due to its robust and rapid growth as well as the similarities of its assembly factors to those of higher eukaryotes [10, 11].

1.2 Ribosome assembly in eukaryotes is a multi-stage process

The mature eukaryotic ribosome contains four ribosomal RNAs (rRNAs) that form the catalytic core of two subunits. These are the 18S rRNA in the small subunit (SSU) and the 25S, 5.8S, and 5S rRNAs in the large subunit (LSU). The rRNAs are associated with ribosomal proteins (r-proteins) that form the remainder of the structure of each subunit. In addition to the complexity of the components of each subunit, both the rRNA and the r-proteins are subject to covalent modifications that alter their function [12]. The assembly of the ribosome in eukaryotes is a multi-stage process facilitated by over 100 protein and non-coding RNA assembly factors [13]. In contrast to the rRNA and r-proteins, assembly factors act transiently upon the ribosomal precursors to facilitate the assembly process but do not comprise a part of the mature subunits [14-16]. Assembly factors compose a set of proteins and RNAs that fulfill various roles within the assembly process. These factors are essential for the proper assembly of the ribosomes as they facilitate regulation, structural chaperoning, and modification of the rRNA and proteins. Due to the complexity of this process, the individual steps of ribosome assembly are highly regulated and progress in a distinct order as controlled by the action of assembly factors. The physical

separation of different stages of ribosome assembly also contributes to the regulation of the process as the subunit precursors progress from the nucleolus to the nucleus and, finally, the cytoplasm [17]. Assembly factors regulate the order of assembly by multiple mechanisms. Assembly factors may occupy sites filled by a different protein in later stages of assembly or prevent a conformational change that cannot proceed until certain checkpoints have been passed. The covalent modification of proteins and rRNAs by assembly factors also serves as a regulatory mechanism within the pre-ribosome. In addition to regulation by assembly factors, the order of assembly is enforced by the availability of factors within the current cellular compartment [18, 19]. Factors that bind during the cytoplasmic stages of ribosome assembly are localized to the cytoplasm and therefore cannot compete with nucleolar factors for binding while the pre-ribosome is within the nucleolus. For instance, the cytoplasmic factor Tsr3 shares a binding site with the factor Rio2. The binding of Tsr3 to the shared site is a regulatory mechanism that prevents the re-association of Rio2 after it was released. The competition with Tsr3 aids the release of Rio2 in the cytoplasm but not in the nucleus, where Tsr3 is not present [20].

The assembly of the ribosome begins in the nucleolus of the cell, a non-membrane-bound organelle that forms around the DNA coding for the rRNA (rDNA) [18, 21]. After completing the nucleolar stages of assembly, the ribosomal precursor is exported to the nucleoplasm and later the cytoplasm once certain assembly checkpoints are passed [16, 17]. In each sub-cellular compartment, the ribosomal precursor is exposed to a new set of factors and r-proteins to facilitate the next stages of its maturation [18, 19]. As a cell can produce multiple ribosomes concurrently, multiple individual stages of the precursor are present within each subcellular compartment. These individual stages can be separated and/or characterized from a mixture via various techniques depending on their properties. For example, single-particle cryo-electron microscopy (cryo-EM) methods have explored the transformation of the precursor within a

subset of highly similar particles isolated based on their association with a particular affinity-tagged assembly factor. This method allows for the isolation of particles that have not undergone the release of a specific factor and can characterize the function of that factor by revealing the stages immediately before and after its function. This isolation is often difficult due to the low quantity of these specific stages of the pre-ribosome within a given cell due to the speed at which each precursor is converted into the following stage. As such, purification strategies often impose artificial conditions that prevent the processing of the pre-ribosome beyond a specific step leading to an accumulation of the pre-ribosomal particle that precedes the blocked step [18, 21]. Expression of mutant forms of assembly factors or strains deficient in those factors often results in disrupted ribosome assembly and the accumulation of a target precursor at higher levels per cell than in non-modified cells [21]. For instance, the mutation of a late-stage small subunit assembly factor known as Ltv1 allows for the purification of otherwise short-lived intermediates. The structural characterization of these intermediates allowed for studies of the spatial interactions formed by Ltv1 with the other components of the pre-ribosome. Additionally, the characterization of subcellular fractionation of the nucleus, nucleolus, and cytoplasm of a single population of cells allows for the characterization of how precursors travel across the cell and the transitions that occur along with these transits [16, 17]. For example, in human cells, the composition of pre-ribosomes exported from the nucleus to the cytoplasm has been characterized by comparing purifications from the nucleus and nucleolus [17]. Human cells are often utilized for these forms of analysis due to the dense layer of heterochromatin surrounding the nucleus, which makes it less prone to disruption during cell lysis compared to the yeast nucleus. The stability of the human nucleus greatly aids in the purification of individual compartments.

1.2.1 Assembly of the ribosome begins co-transcriptionally with the nucleolus

The order in which assembly factors act within each subcellular compartment is further regulated. The initial transcription of the rDNA into an rRNA precursor forms the first stage of the assembly process [22]. The 35S rRNA precursor, which contains the 18S, 5.8S, and 25S rRNAs that will form the mature ribosome ribosomal subunits [23, 24], is transcribed by RNA polymerase I (PolI). The individual rRNAs are separated from each other within the 35S rRNA precursor by a set of internally transcribed spacers (ITS1 and ITS2) and are flanked on the 5′ and 3′ ends of the 35S rRNA precursor by externally transcribed spacers (5′ETS and 3′ETS) [22]. These spacer regions must be removed for the mature subunits to be properly formed. The spacer regions serve as essential binding sites for assembly factors and, therefore, cannot be removed prior to specific assembly events [25-27]. Transcription of the 35S rRNA precursor occurs within the nucleolus. During the transcription of this precursor, assembly factors and r-proteins bind the growing rRNA as binding sites are revealed. These factors serve in turn to recruit other factors either concomitantly or at a later stage. Many sets of factors form stable complexes that bind the growing precursor as protein or ribonucleoprotein (RNP) complexes [25, 28-30]. In the cases of these complexes, only one binding event of a complex component is necessary to facilitate the joining of the complex to the growing pre-ribosome [25]. These complexes and the individual factors that bind the precursor serve a diverse array of roles. Some serve as structural scaffolds for the correct folding and re-folding of the rRNA and assembly of the r-proteins. These chaperoning factors act both to ensure that regions of the precursor can adopt their mature conformation as well as to temporarily hold the precursor in an immature state to allow for the further binding of other assembly factors before the precursor proceeds [25, 31].

Other assembly factors serve catalytic roles that covalently modify the rRNA or cleave the spacer regions to facilitate the progression of the 35S precursor into the mature 18S, 5.8S, and

25S rRNAs [32]. Throughout ribosome assembly, the rRNAs collectively undergo over 100 post-transcriptional modifications wherein individual nucleotides are modified by adding covalently attached groups or converted to structural isomers. Many of these processes are catalyzed by standalone modification enzymes such as Nop2, the enzyme that introduces methyl groups to cytosines at specific locations in the large subunit [33]. Other modifications are carried out by complexes of modification enzymes that can target many sites across multiple RNAs based on the base pairing interactions of the guide RNAs to which these protein complexes are bound. These guide RNAs fall into two categories of small nucleolar RNA (snoRNA) [12]. These categories are the H/ACA snoRNAs and the C/D box snoRNAs. The H/ACA snoRNAs typically consist of small RNAs that bear two hairpins separated by the hinge (H) region and bear a terminal box containing the sequence ACA. Each of these hairpins serves to guide a set of proteins in the pseudouridylation of RNA that bind the upper region of internal loops within the hairpins [34]. In the function of a canonical H/ACA snoRNP, a target RNA binds the upper portion of the internal loop of a hairpin which frames a uridine base for conversion into a pseudouridine. This conversion is catalyzed by Cbf5, a protein that binds H/ACA guide RNAs. Cbf5, Nop10, Gar1, and Nhp2, are known as the canonical H/ACA proteins. Post-transcriptional modifications of RNA and post-translational modifications of proteins can serve as regulators of the assembly process, with modifications affecting the binding or release of specific factors [22, 24, 35]. Additionally, modifications have effects on the function of the mature ribosome, and deficiencies in a modification can affect the process of translation once the precursor has matured and entered the pool of active ribosomes [8].

Another role of assembly factors is the cleavage of the pre-rRNA spacer regions. Because of its transcription as a single unit, the rRNA precursor requires multiple cleavage events to separate the individual 18S, 5.8S, and 25S rRNA transcripts by the removal of the spacer regions [36]. The cleavage sites responsible for the proper formation of the small subunit are labelled A_0, A_1,

A_2, and A_3. Sites A_1 and A_2 are found within the 5′ETS region, and sites A_2 and A_3 are found within the ITS region. The endonucleolytic cleavages at sites A_0 and A_1 remove the 5′ETS regions from the 18S rRNA, while the cleavages at sites A_2 and A_3 separate the 18S rRNA from the remainder of the precursor, including the majority of the ITS1 region [18, 22]. The final maturation of the 18S rRNA also includes an exonucleolytic removal of a small portion of the ITS1 region that remains after the A_2 cleavage [36]. The initial cleavages at sites A_0, A_1, and A_2 occur while the rRNA precursor resides within the nucleolus, but the final trimming of the ITS1 remnant occurs after the small subunit precursor has been exported to the cytoplasm [32, 36].

1.2.2 snoRNPs act as essential assembly factors at specific stages of assembly

The cleavages of the spacer regions surrounding the 18S rRNA are dependent on the activity of a wide array of assembly factors that bind across multiple regions of the rRNA precursor. The 18S rRNA can be further divided into regions based on the regions of the small subunit they will eventually form [28, 31, 37]. These regions are known as the 5′ domain, central domain, 3′ major domain, and 3′ minor domain [22] (Figure 1). The 5′ and central domains form the body and platform of the mature SSU, while the 3′ major and 3′ minor domains will go on to form the head and beak [13]. Each of these regions, along with the 5′ETS and the ITS1, are associated with a set of assembly factors and r-proteins that bind as the section is transcribed. These sets of assembly factors often form stable complexes that remain assembled when not interacting with the rRNA precursor and further interact in complex networks with the other complexes, assembly factors, and r-proteins while they are bound to the pre-ribosome [38]. Whereas many assembly factors bind immediately as the corresponding binding sites along the rRNA are transcribed, some also bind as processing events and conformational changes reveal binding sites within previously transcribed domains [29, 31]. Of the assembly factors that bind co-transcriptionally, a particularly noteworthy set is the ribonucleoprotein complexes that form around the 3 essential snoRNAs: U3, U14, and snR30. These RNAs are small nucleolar RNAs

of the C/D box (U3, U14) and H/ACA (snR30) families. Whereas snoRNAs typically serve to guide RNP complexes to sites on RNA where post-transcriptional modification occurs, these three RNAs serve essential roles instead of or in addition to the canonical role as a modification guide [27, 30, 39].

The U3 snoRNP particle binds the earliest of the three essential snoRNAs. It binds during the transcription of the 5′ETS (Figure 1). In particular, the complexes UtpA and UtpB form interactions with the 5′ETS, the U3 snoRNP, and other assembly factors. These complexes include structural proteins as well as enzymes that facilitate rRNA processing. While several proteins bind along with U3 during this stage, other proteins that can interact with the U3 snoRNP complex are recruited during later parts of transcription [28, 40]. Together with these proteins, U3 forms a structural scaffold for the small subunit precursor during the early stages of its assembly and is essential for the proper formation of the central pseudoknot region of the SSU.

Along with the protein complexes UtpA and UtpB and several individual factors, the U3 snoRNP forms a complex known as the 5′ETS particle [25, 27, 38]. The 5′ETS particle is a complex that facilitates the binding of the U3 snoRNA to the 5′ domain of the 18S rRNA, where it serves as a chaperone for the proper folding of the region. In addition, the binding of the 5′ETS particle is also essential for the positioning and recruitment of processing assembly factors such as Utp24, a nuclease that binds the U3 snoRNP and is responsible for the cleavages at sites A_1 and A_2, which separate the 5′ETS and ITS1 spacers from the 18S rRNA.

The second essential processing RNA to bind the ribosomal precursor is U14 (Figure 1). U14 is a C/D box snoRNA with multiple functions. U14 targets a region of the large subunit precursor for 2’O-ribosome methylation. This interaction is accomplished in the typical fashion for a box C/D snoRNA, with the snoRNA positioning the base for modification by the protein components of the RNP [41].

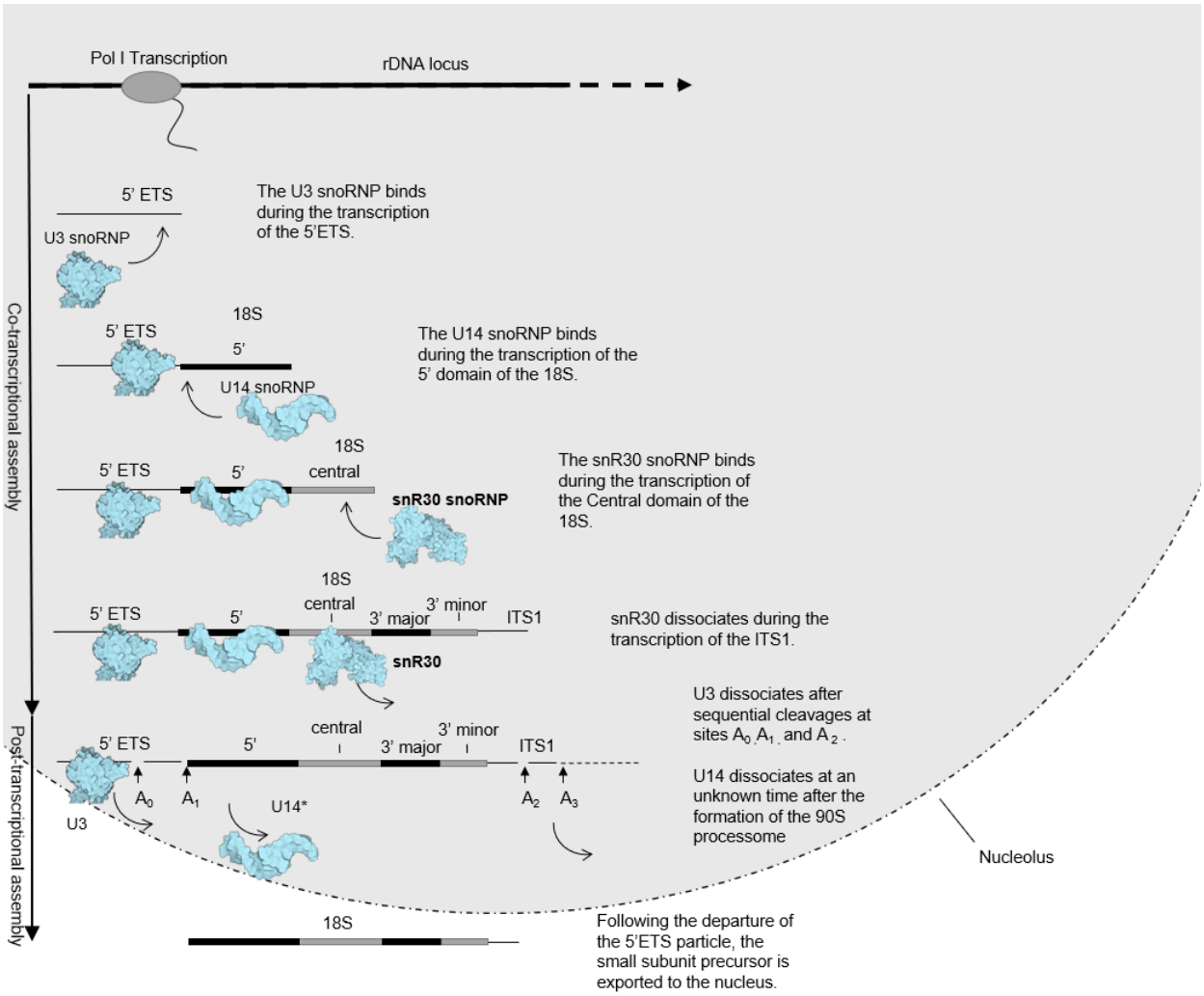

Figure 1: Transcription of the rRNA precursor in yeast with the association and dissociation of the three essential snoRNPs involved in small subunit assembly, U3, U14, and snR30. The association of the U3 snoRNP occurs during the transcription of the 5′ETS, and it remains stably bound until the cleavage of A_0, A_1, and A_2 occurs. The U14 snoRNA binds during the transcription of the 5′ domain of the 18S rRNA and remains bound until the transcription of the ITS1 region. The exact timing of U14 dissociation remains unclear. snR30 binds during the transcription of the central domain of the 18S rRNA and dissociates during the transcription of the ITS1 region. snoRNPs are represented schematically as their molecular structure is not known.

However, the cell is not dependent on this U14-mediated modification, as inhibiting the modification does not introduce a lethal phenotype [41]. The second function of U14 is connected to its binding across the 5′ domain of the 18S rRNA. While it has been shown that this binding and the presence of U14 are required for proper small subunit assembly, little is known about the exact mechanism of U14 and its associated proteins [30, 41].

The final essential RNA assembly factor is snR30. snR30 bears the H and ACA box elements typical of an H/ACA snoRNA but has no known sites of pseudouridylation [42] (Figure 2). snR30 also binds the typical H/ACA proteins Cbf5, Nop10, Gar1, and Nhp2 but binds the rRNA in an incorrect orientation to facilitate pseudouridylation [30, 43]. While its binding site and several features of its associated proteins have been characterized, there remains no consensus as to the exact mechanism for snR30 function and the reason that it is essential.

A feature that is common between all three essential snoRNAs is the fact that the depletion of any of these snoRNAs results in an inability of the cell to cleave the A_0, A_1, and A_2, sites of the rRNA precursor [30, 42, 44]. These cleavages are of particular importance as they serve to separate the spacer regions from the growing pre-ribosomal particle, and without them, the pre-ribosome is incapable of progressing onwards to the next stage of the assembly. These cleavages occur within a metastable precursor of the pre-ribosome known as the 90S precursor or 90S processome. Due to the stability of this complex and the importance of these cleavages, many analyses have been made of this particle [31, 37, 45].

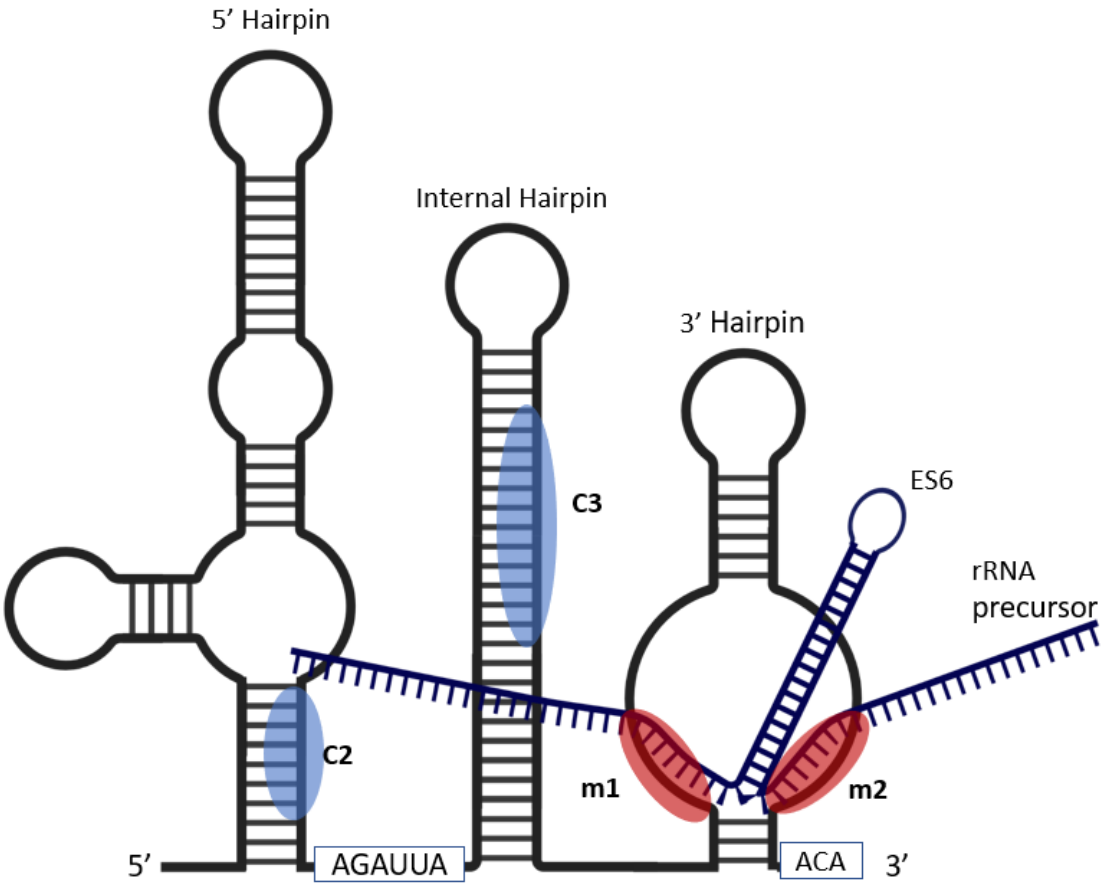

Figure 2: Main structural features of the snR30 snoRNA bound to the rRNA precursor (blue). Shown are the major structural features of the snR30 RNA: the 5′ hairpin, the internal hairpin, and the 3′ hairpin. The H and ACA boxes are labelled, and the non-essential binding regions (C2 and C3), where snR30 interacts with rRNA, are highlighted in light blue. The essential binding regions of the 3′ hairpin, m1 and m2, are highlighted in red. Minor structural features of the 5′ hairpin and internal hairpin, including bulges, are omitted.

After the formation of the 90S particle and the changes associated with the cleavage of the 5′ETS, U3 dissociates as a part of a large RNP particle known as the 5′ETS particle. Components of the 5′ETS particle can be recycled and reassembled onto a new pre-ribosome after dissociating from the 90S particle. While the exact time of dissociation for U14 is unknown, it also dissociates after the formation of this intermediate and dissociates before the export of the small subunit precursor to the cytoplasm [28] (Figure 1). The timing of the dissociation of snR30 is more precisely known from analyses of the co-transcriptional stages that precede the

cleavage events [28]. snR30 is present in ribosomal precursors up to those containing the central and minor domains. snR30 is detected in lower amounts in those ribosome precursors containing the minor domain and is fully absent once the ITS domain has been transcribed (Figure 1) [28].

1.3 snR30 is an essential and unusual H/ACA snoRNA

The H/ACA snoRNA family is a subset of small nucleolar RNAs that are characterized by conserved elements. The H and ACA boxes are highly conserved across the H/ACA family, as are the “core” H/ACA proteins Cbf5, Nop10, Gar1, and Nhp2 [46]. These proteins form a snoRNP with a specific H/ACA RNA that base pairs to a target RNA and positions Cbf5 for the conversion of uridine to a pseudouridine [34]. Despite containing an H and an ACA box (Figure 2) and binding all of the core proteins, snR30 has no known sites for pseudouridylation [47]. The interaction of snR30 within the SSU precursor is the only known role for this RNA. The structure of snR30 consists of three main hairpins: the 5′ hairpin, the internal hairpin, and the 3′ hairpin (Figure 2) [30, 42]. Of these hairpins, only the 3′ hairpin is essential for the function of the snoRNA. The 5′ and internal hairpins of snR30 can be removed without abolishing the function of the snoRNA. There are two potential rRNA binding sites that reside on these hairpins that may have non-essential roles in the function of snR30 [30, 42]. This is supported by comparisons to the human homolog of snR30, U17, which bears high similarity in the 3′ hairpin but lacks an equivalent region to the 5′ hairpin [42]. Crosslinking and mutational studies have shown that the main binding sites of snR30 (m1 and m2) reside within the 3′ hairpin along the lower sections of the internal loop within the 3′ hairpin [30, 42] (Figure 2). This is contrasted to the binding of a typical H/ACA snoRNP, which occurs along the upper portion of an internal loop and is essential for framing the target uracil for pseudouridylation [34]. The binding sites of snR30 are referred to as the m1 and m2 sites, and the corresponding binding targets within the rRNA precursor are labelled rm1 and rm2, respectively (Figure 2). This set of binding sites is

also collectively referred to as C1 to differentiate it from the two other potential regions: C2 and C3 [30] (Figure 2). snR30 is a conserved RNA across eukaryotes and shows a high degree of conservation within the essential region. While the 5′ and internal hairpins do not have structural homologs within the human equivalent, U17, the binding of the m1 and m2 regions within an essential hairpin loop is conserved, as reviewed in [48]. Furthermore, in humans, the binding of U17 to the Cbf5 homolog dyskerin is of interest due to the role that dyskerin plays in the development of Dyskeratosis congenita. While Dyskeratosis congenita is generally associated with the role dyskerin plays in the maintenance of telomeres, it is possible that the development of ribosomopathies is linked to dyskerin's role as part of the U17 snoRNP as reviewed in [49].

1.3.1 snR30 binds at sites rm1 and rm2 within the central domain

Crosslinking analysis of RNA-RNA interactions is a powerful tool in the determination of the binding site of ribosomal assembly factors and the composition of subsets of RNPs. [30, 50, 51]. Using this analysis, coupled with mutational analysis of snR30, it has been identified that snR30 binds primarily and essentially with the m1 and m2 regions of its 3′ hairpin (Figure 2). These regions bind to expansion segment 6 (ES6) of the 18S rRNA precursor [30, 42]. This region is not well resolved in the existing high-resolution structures of the late nucleolar ribosome precursor wherein the cleavage events at A_0, A_1, and A_2 take place (90S particle or the 90S processome) but is suggested to be involved in the structural rearrangement that occurs during A_1 cleavage [37]. The binding of snR30 to the rm1 and rm2 sites is non-compatible with the folding of this domain into the conformation found within the mature ribosome. This is due to the fact that the binding sites are involved in the formation of two hairpins within the mature rRNA that cannot form while snR30 is interacting at the rm1 and rm2 sites. This binding indicates that sn30 must dissociate prior to the structural rearrangement that serves to bring ES6 into its mature conformation. Furthermore, it is known that the binding of snR30 to rm1 and rm2 is the

dominant contributor to the binding of snR30 based on *in vitro* assays measuring the affinity of snR30 truncations to rRNA fragments [52].

1.3.2 snR30 interacts in a transient manner and dissociates prior to the essential cleavages

The direct function of assembly factors such as snR30 is difficult to ascertain due to the transient nature of their association with the pre-ribosome. Analysis of the co-transcriptional stages of ribosome assembly has shown that snR30 is both the last of the essential snoRNAs to bind and the first to dissociate, being undetectable in particles that contain any portion of the ITS1 [30]. Contrasted to this time frame, the cleavages of $A_{0,}$ $A_{1,}$ and $A_{2,}$ occur after the ITS1 region has been transcribed and take place within a well-characterized metastable 90S particle [53]. Given this timing, snR30 is hypothesized to have an effect on the early, less stable intermediates that cascades to an essential part of the cleavage events occurring within the 90S particle [18]. The structure of the 90S particle has been well resolved to the extent that the states immediately prior to and after the A_1 cleavage have been observed at 3.2-angstrom resolution [18, 53]. Characterization of this particle has shown that there is a distinct shift of the 5′ETS region and the associated assembly factors towards the central domain. In particular, the nuclease UTP24 is in close proximity to ES6. However, the direct interactions are not easily determined due to a lack of resolution at ES6 in these structures [18, 37]. Due to this, the binding site of snR30 is not visible, regardless of the fact that snR30 is not expected to be bound to this particle.

RNA-RNA binding between snR30 and the rRNA precursor forms part of a larger network of binding that comprises snR30 and several protein assembly factors. snR30 is known to bind the canonical H/ACA proteins (Cbf5, Nop10, Gar1, and Nhp2), the helicases Rok1 and Has1, the PIN domain protein Utp23, and two small subunit proteins, Rps9 and Rps18 [30, 43, 44, 54]. The interacting proteins of snR30 have been characterized by pulldown assays [43] as well as *in vitro* binding assays [52]; however, the extent to which snR30 binds specific proteins during

its association with the SSU precursor cannot be fully ascertained based on these assays. Rok1 is a protein of interest in studies of snR30 due to the requirement for its helicase activity to separate snR30 from the pre-rRNA [30]. The fact that snR30 must be released by the activity of a helicase is a feature shared by the other essential assembly snoRNAs but not a feature typical of canonical H/ACA snoRNAs [34, 44].

The essential nature of snR30 means that both the RNA itself and the associated proteins that make up its RNP are of interest to better understand how it mediates ribosome assembly. This analysis is complicated by the fact that snR30 binds only a few ribosomal precursors. Due to the highly transient binding of snR30, purifications of pre-ribosomes isolate predominantly snR30-free states. Additionally, the states to which snR30 does bind are not highly stable compared to mature ribosomes or metastable intermediates such as the 90S particle (Figure 1) [28, 37, 40]. The dissociation of snR30 from the ribosomal precursor occurs during the transcription of the ITS1 region [28]. While it is unknown if snR30 dissociates individually or as part of a larger snoRNP at this point, two proteins, Utp23 and Rok1, are known to be essential for its release from the pre-ribosome.

1.3.3 The overall mechanism of snR30 is unknown, although certain interactions of snR30 within the precursor have been characterized

The identified assembly factors found to bind snR30 give some insight into the potential functions of this snoRNA. The assembly factor Utp23 interacts with snR30, which is of particular note due to the potential for this protein to facilitate further interactions within the pre-ribosome. snR30 has not been shown to have any direct interaction with the nuclease responsible for A_1 and A_2 cleavage, which is Utp24 [32, 53]. Utp23 is a known interaction partner of Utp24 based on crosslinking assays [55]. The same assays also show Utp23 binding Nhp2 and Rok1, both of which are known to associate with snR30 as well as another ribosome biogenesis factor, Rrp7.

This data on snR30, in combination with the existing information on the cleavage of sites $A_{0,}$ $A_{1,}$ and $A_{2,}$ has led to a set of two non-exclusive hypotheses proposed by the Kothe group on the function of snR30 [48]. The first hypothesis revolves around the binding of snR30 at site rm1 and rm2 as an essential regulatory event to prevent the premature folding of the 18S rRNA into its mature state. This would implicate snR30 as a chaperone for the correct folding of rRNA within the ribosome precursor to allow for certain interactions to form or factors to be recruited that cannot efficiently do so once the rRNA has adopted its mature ES6 fold. Alternatively, or additionally, it is theorized that the binding of snR30 serves as a recruitment factor and scaffold for the binding of other assembly factors that form the necessary network for cleavage to take place. In this theory, the association of snR30 would encourage the binding and correct positioning of proteins factors such as Utp23 within the pre-ribosome that allows for the eventual positioning and activation of endonucleases including Utp24 This theory is supported by the binding of Utp23 to snR30 and the subsequent interactions Utp23 with Utp24 [18, 30].

1.4 Pulldowns of SSU intermediates reveal snR30 bound states

A major source of information about the binding and dissociation of snR30 to the active pre-ribosome is based on pulldowns of specific stages of the pre-ribosome. Pulldowns of the pre-ribosome are typically accomplished using a combination of two strategies that solve the two largest hurdles in this analysis. The first of these hurdles is the difficulty of purifying the ribosomal precursor from a cellular environment which contains many complex components that must be separated away. The second is separating specific stages of the pre-ribosome from each other. Without the separation of highly similar ribosomal precursors, timelines of specific changes are difficult to establish, and short-lived particles cannot be isolated due to their low abundance relative to other precursors. This short lived nature of many pre-ribosomal intermediates is contrasted to the mature ribosome which has a half life in the hundreds of hours, with half lives being over 800 hours in some cells [56].

For example, purifications of late stages of the pre-ribosome have been accomplished by the use of cells that are deficient in the production of Fap7, which regulates transition into a quality control intermediate, or deficient in the production of Rio1, which regulates exit from the same quality control intermediate [20]. Either of these two genotypes results in an accumulation of the latest precursor state that the cell can produce without the transition mediated by that assembly factor. This accumulation of a specific precursor solves the second hurdle. By creating an abundance of each precursor, the resulting purifications were able to isolate that precursor from similar, earlier precursors. Each of these depletions was co-expressed with a tandem affinity purification (TAP) tagged variant of an assembly factor known to be bound to that intermediate [20]. The usage of a TAP tag allows for two stages of affinity chromatography to be used, which allows for a highly specific purification. The combination of enrichment of a specific stage of assembly by accumulation and tandem affinity purification allowed for an in-depth analysis of specific stages and a determination of the function of the Rio1 protein during the transition [20].

A similar strategy has been utilized to study the co-transcriptional stages of ribosome assembly with even greater precision. Due to the nature of the co-transcriptional process, the expression of a truncation of the ribosomal RNA results in an accumulation of the corresponding precursor [28, 40]. Analysis of these particles by pulldown, mass spectrometry, and Northern blot has revelated a map of which factors are present across the transcription of each of the domains of the SSU precursor and at several intermediate steps between domains. Pulldowns of the complexes enriched by these truncations were achieved using a two-step purification process. The initial stage was accomplished using a set of MS2 protein-binding RNA aptamers attached to the 3′ or 5’ ends of the truncated rRNA [28, 40, 57]. This purification exploits the affinity of the MS2 binding aptamer for the MS2 coat protein and uses variants of this protein to allow the binding of the RNA to a chromatography resin. Some differences in the effectiveness of the purification were found based on the location of the tag, with 3’ tagged variants of the precursor

performing better in purification of some precursors and the 5’ tag performing better for others [28]. Despite these differences, the use of a 3’ tag has been shown to allow for the purification of all stages of the small subunit precursor [40]. A commonly used variant of the MS2 protein contains a hexahistidine tag, allowing for binding to a nickel sepharose resin and elution with imidazole. Another commonly used variant is an MS2 protein fused to a maltose-binding protein, allowing for the binding of the protein and the accompanying RNA to a dextrin sepharose resin and elution with free maltose [58]. The specificity of the purification was improved by combining the affinity chromatography based on the binding of the MS2-tagged rRNA with further affinity chromatography targeting a TAP-tagged assembly factor.

For the TAP-tagged assembly factors, the authors utilized stably bound factors that are present throughout the vast majority of the ribosome assembly process. Using mass spectrometry and Northern blotting analysis, the protein and RNA composition of each specifically purified stage could be analyzed [28, 40]. This includes the detection of snR30 in complexes arising from the truncation of the rRNA precursor to the central domain of the 18S rRNA, as well as those pre-ribosomes that also contain the 5′ major and 5′ minor domains. However, snR30 is no longer detected once the ITS1 region has been transcribed. This analysis gives some insight into the binding of snR30 to the pre-ribosome but does not enrich for snR30 within stages where snR30 may not be stably bound. With a purification focused more specifically on enriching for snR30, more revealing methods of analysis such as cryo-EM could be performed. These analyses, as well as a comparison of particles enriched for snR30 to those without, will be able to answer further questions surrounding the activity of snR30. In particular, the answers to how snR30 affects the binding of factors and folding around the binding site at ES6 can be answered in greater clarity using purifications of the pre-ribosome with specificity for those states to which snR30 is bound.

Chapter 2: Objectives

In order to characterize snR30 with respect to its role in the structure, composition, and regulation of the growing pre-ribosome, it is necessary to produce a system wherein snR30 is isolated in complex with the pre-ribosome at distinct stages of the process of ribosome assembly. This isolation must meet several thresholds for the analysis of the resulting particles to be considered successful. This purification will allow for the comparative analysis of the behaviour of snR30 in complex with the earliest pre-ribosome stages that it binds, relative to the later pre-ribosome stages that snR30 binds. Comparison of complexes lacking snR30 to those that contain snR30 will also be informative as an indicator of the role of snR30 across the timeline of its association. In order for this analysis to be successful, amounts of the target pre-ribosome complex must be produced that are sufficient for the analysis of the composition of the pre-ribosome by Northern blotting and mass spectrometry. In addition to the purification of a sufficient amount of material to conduct these analyses, the particles must also be purified to sufficient homogeneity so that the protein and RNA composition differences between them can be reliably resolved. Additionally, in order for the structural changes mediated by snR30 to be determined, the system must produce a sufficient amount of snR30-bound pre-ribosomes for the analysis of the particle by high-resolution cryo-EM. While cryo-EM requires less overall material than other analyses due to the low volumes utilized, the level of structural homogeneity of the particles must be high enough for image acquisition of many instances of each particle[37].

To accomplish the goal of purifying snR30 in a ribosome-bound state, I engineered a set of *S. cerevisiae* strains capable of expressing MS2 aptamer-tagged rRNA truncations under the control of the Gal1 promoter. This system is closely based on the establishing work for purifications of specific, co-transcriptional stages of the pre-ribosome [28, 40]. These strains are also expressing functional snR30 tagged with a tobramycin binding aptamer allowing for a

tandem RNA aptamer affinity purification of the snR30 bound pre-ribosome. I conducted a set of 11 iterative test expressions and purifications of these strains in order to optimize the ideal expression, cell lysis and purification conditions required to produce a homogenous population of precursors in amounts sufficient for the analysis of the complex via cryo-EM and mass spectrometry. In addition to determining the required growth volume and densities for the cells, I optimized the buffer conditions of the individual maltose binding resin purification of pre-ribosomes and the subsequent enrichment of snR30 bound instances using tobramycin affinity chromatography. Over the course of these purifications, I identified a set of buffers that allows for the purification of sufficient amounts of particles for analysis with a level of homogeneity that predicts the feasibility of structural analysis. I further identified that inconsistent amounts of product purified during the tobramycin affinity purification were a major limiting step in the utilization of this purification system for the determination of the role of snR30 across the nucleolar stages of small subunit assembly in eukaryotes.

Chapter 3: Materials and Methods

3.1 Materials

YNB + Nitrogen and SC-His-Leu dropout mix for selective yeast media were purchased from Sunrise Science Products. Stain and grids for negative stain electron microscopy were purchased from Electron Microscopy Sciences, and dextrin sepharose resin from GE Healthcare. NP-40 was obtained from Millipore Sigma under the brand name Igepal-C630. Raffinose, tobramycin, galactose, and Miniprep DNA Extraction Kit are Biobasic products. The enzymes Q5 DNA polymerase, T7 DNA ligase, NEB5 alpha competent *E. coli* cells, and AMV reverse transcriptase, as well as their corresponding buffers, were purchased from New England Biolabs (NEB). Oligonucleotides were ordered from Integrated DNA Technologies (IDT), and all other reagents, including enzymes and corresponding buffers, were obtained from Thermo Fisher. Rosetta DE3 cells containing pHMM were previously prepared in our lab from Rosetta DE3 competent cells obtained from Millipore Sigma and pHMM, which was a gift from Robert Batey & Jeffrey Kieft (Addgene plasmid # 67717). YDU1 cells (Table 1) were produced in the Knop Lab at the University of Heidelberg, and the strains YDU1-central, and YDU1-major were prepared previously in our lab by the transformation of YDU1 cells with pESC-Leu-central and pESC-Leu-major plasmids, respectively.

Table 1: List of strains utilized in this thesis

Strain Name	Parent strain	Genotype	Description	Plasmids
BY4741	S288C	MATa, his3Δ1 leu2Δ0, met15Δ0, ura3Δ0,	Basic laboratory strain	N/A
YDU1	BY4741	TetR-KanMX:snR30	A modified BY4741 strain containing the Tetracycline responsive element inserted into the snR30 promoter along with a KanMX selectable marker	N/A
YDU1-snR30L	YDU1		YDU1 containing a vector for the expression of snR30	pRS313-snR30L
YDU1-5′Tob	YDU1		YDU1 containing a vector for the expression of snR30 with a 5′ hairpin tobramycin J6f1 aptamer	pRS313-snR30L-5′Tob
YDU1-Central	YDU1		YDU1 containing a vector for the inducible expression of a tagged variant of the 35S rRNA truncated to the central domain of the 18S rRNA	pESC-Leu-central
YDU1-Major	YDU1		YDU1 containing a vector for the inducible expression of a tagged variant of the 35S rRNA truncated to the Major domain of the 18S rRNA	pESC-Leu-Major
YDU1-Central-5′Tob	YDU1		YDU1 containing plasmids for the expression of tagged variants of snR30 and an rRNA truncation to the Central domain	pESC-Leu-central, pRS313-snR30L-5′Tob
YDU1-Major-5′Tob	YDU1		YDU1 containing plasmids for the expression of tagged variants of snR30 and an rRNA truncation to the Major domain	pESC-Leu-Major, pRS313-snR30L-5′Tob

3.2 Mutagenesis of pUC19-snR30L-5′Tob

The addition of a tobramycin binding aptamer to the 5′ hairpin of snR30 was accomplished using insertional mutagenesis with a previously prepared plasmid called pUC19-snR30L containing

the snR30 coding sequence with endogenous promoter and terminator (snR30L). pUC19-snR30L was used as a template and subjected to PCR-based mutagenesis with the following conditions. 0.66 ng/μL of template was combined with 0.04 U/μL of Q5 DNA polymerase in 1x Q5 reaction buffer (NEB). The mixture was supplemented with 2.5% DMSO, 200 μM dNTPs, and 0.5 μM of primers snR30-5′Tob-sense and snR30-5′-antisense (Table 2). The DNA was denatured at 98 °C for 30 seconds, followed by 30 cycles of: at 98 °C for 10 seconds, 65 °C for 30 seconds, and 72 °C for 120 seconds. The final extension at 72 °C occurred for an additional 2 minutes. The PCR reaction was then incubated with 0.05 U/μL of DpnI in 1x TANGO buffer (Thermo Fisher) for 1 hour at 37 °C.

Following mutagenesis and DpnI digestion, the plasmids were re-circularized by the addition of 0.5 U/μL of T4 DNA ligase and 1x DNA ligase buffer (NEB). The ligation mixture was incubated at 16 °C for 1 hour and then transformed into NEB5alpha HE competent *E. coli* cells (NEB) using the manufacturer's protocol and plated on LB agar containing 100 μg/mL ampicillin. A single colony was selected and grown in 10 mL LB containing 100 μg/mL ampicillin and plasmid DNA extracted using a miniprep kit (Biobasic) according to the manufacturer's protocols. Extracted pUC19-snR30L-5′Tob plasmids were screened by Sanger sequencing.

3.3 Insertion of snR30L-5′Tob into pRS313

pUC19-snR30L-5′Tob was used as a template for the amplification of snR30L and the inserted 5′-hairpin tobramycin aptamer. 0.72 ng/μL of the template was combined with 0.03 U/μL of PFU polymerase in 1x PFU buffer (Thermo Fisher) along with 2% DMSO and 200 μM dNTPs. Primers snR30-promoter-sense and snR30-terminator-antisense were included at 0.5 μM (Table 2).

Table 2: List of Oligonucleotides and their use

Oligo	Sequence 5′-3′	Use
snR30 promoter sense	CTGTAAATTGCTCTTACTACAAACCTGC	Amplification of the snR30 gene
snR30 terminator antisense	CATGAAGTGGGCCAAGGGAATTAAGAG	Amplification of the snR30 gene
snR30-5′-antisense	Phos-GATCAGAGGAGAAGTCAGGAGC	Insertional mutagenesis
snR30-5′-Tob-sense	GCGTCGGCACGAGGTTTAGCTACACTCG TGCCATCGATGATCAGAGTTTTGAGTCGT CAGAC	Insertional mutagenesis
Tob tag antisense	GGCACGAGTGTAGCTAAACCTCGTTCCG	cDNA generation and amplification for RT-PCR
snR30 RTPCR sense	CATAGTCTCGTGCTAGTTCGGTACTATA CAGGG	Amplification of cDNA for RT-PCR
4xMS2 XhoI antisense	GAGCTCGAGACATGCATG GG	cDNA generation and amplification for RT-PCR
rRNA central RTPCR sense	CATCGTAATGATTAATAGGG	Amplification of cDNA for RT-PCR
Major-RTPCR-sense	CGAGGAATTCCTAGTAAG CG	Amplification of cDNA for RT-PCR

The reaction was denatured at 98 °C for 30 seconds, followed by 30 cycles of: 98 °C for 10 seconds, 54 °C for 30 seconds, and 72 °C for 120 seconds. An additional 5-minute incubation at 72 °C was used to facilitate the final extension. The PCR reaction was then incubated with 0.05 U/ μL of DpnI in 1x TANGO buffer (Thermo Fisher) for 1 hour at 37 °C.

Approximately 400 ng of pRS313 plasmid was digested by 0.05 U/μL SmaI in 1x TANGO buffer (Thermo Fisher) for 1 hour at 25 °C. The digested plasmid was combined with digested PCR product at a 5:2 v/v ratio along with 0.025 U/μL SmaI, 10% PEG 4000, and 0.5 U/μL of T4 DNA ligase in 1x DNA ligation buffer. Following 16 hours of incubation at 19 °C, the mixture was used to transform NEB5alpha HE competent *E. coli* cells using the manufacturer's protocol. Transformants were plated on LB medium containing X-Gal and 100 μg/mL ampicillin. The resulting colonies were screened by the selection of white colonies.

Table 3: List of plasmids utilized in this thesis

Plasmid	Backbone	Insert	Insertion site
pRS313-snR30L	pRS313	snR30 gene	SmaI
pRS313-snR30L-5′Tob	pRS313	snR30 gene with a tobramycin J6f1 aptamer inserted to replace nt 235-239	SmaI
pESC-Leu-ITS1-4xMS2	pESC-Leu	RDN37-1 rDNA locus truncated to the end of RDN18-1, with a 4xMS2 aptamer sequence at the 3′ end	SalI and XhoI
pESC-Leu-Central-4xMS2	pESC-Leu	RDN37-1 rDNA locus truncated to nucleotide 1837 with a 4xMS2 aptamer sequence at the 3′ end	SalI and XhoI
pESC-Leu-Major-4xMS2	pESC-Leu	RDN37-1 rDNA locus truncated to nucleotide 2330 nt with a 4xMS2 aptamer sequence at the 3′ end	SalI and XhoI

3.4 Yeast transformations

S. cerevisiae competent cells of the strains YDU1, YDU1-central, and YDU1-Major (Table 1) were prepared by harvesting 50 mL of cells grown to an optical density at 600nm (OD_{600}) of 1 in YPD or SC-Leu as appropriate by centrifugation at 5000 × *g* for 5 minutes in a Multifuge x3r centrifuge (Thermo Fisher) with a bioshield 1000A rotor. The cells were washed in sterile distilled de-ionized water, followed by washing in sterile SORB buffer (100 mM LiOAc,10 mM Tris-HCl pH 8.0, 1 mM EDTA, 1 M sorbitol). Cells were re-suspended in 360 μL SORB buffer, and 10 μL aliquots were stored at −80 °C until use.

Aliquots of competent YDU1 cells were combined with of pRS313-snR30L-5′Tob plasmid to a concentration of 5 ng/μL and ssDNA from salmon testes (Thermo Fisher) to a concentration of 5 μg/μL. Aliquots were then combined with a six-fold volume of PEG solution (100 mM LiOAc,10 mM Tris-HCl pH 8.0, 1 mM EDTA, 40% PEG 3350) and incubated at room temperature for 30

minutes. The mixture was supplemented with DMSO to a final concentration of 10% and heat shocked at 42 °C for 20 minutes. Cells were washed and re-suspended in YPD medium before being plated on SC-Leu or SC-His-Leu agar plates with 2% glucose prepared using YNB + nitrogen and SC-Leu dropout mix supplement, or SC-His-Leu dropout mix supplement (Sunrise Science Products). Successful transformants were re-plated on selective medium to confirm growth. Individual colonies were grown in SC-His-Leu liquid medium, diluted in an equal volume of 30% sterile glycerol, and stored at −80 °C.

3.5 Purification of Histidine-MBP-MS2 protein

To facilitate the binding of MS2 aptamer-tagged RNAs to a chromatography resin, fusion proteins of the MS2 coat protein with easily purifiable proteins have been designed. The histidine-MBP-MS2 (HMM) protein is a fusion protein of the MS2 coat protein and maltose-binding protein (MBP). This allows the protein to bind both the MS2 aptamer and maltose-based resins. The protein also contains a hexahistidine tag which allows binding to nickel sepharose resins. To purify this protein for use in the purifications of MS2-tagged RNAs, I utilized Rosetta DE3 *E. coli* cells containing the pHMM plasmid for the expression of HMM [59]. These cells were inoculated in 2 L of LB medium containing 50 μg/mL kanamycin. The cells were grown at 37 °C with shaking from an initial OD_{600} of 0.086. Once the cultures had reached an OD_{600} of 0.5, they were induced by the addition of IPTG (Biobasic) to a final concentration of 1 mM. Three hours post-induction, the cells were harvested by centrifugation at 5000 × *g* for 15 minutes at 4 °C in a Sorval Lynx 6000 centrifuge (ThermoFisher) with a Fiberlite F9 6x1000 rotor. The cells were stored at −80 °C after being shock frozen in liquid N_2. The frozen pellet was thawed on ice and resuspended in 5 mL/g Ni^{2+} buffer A (20 mM Tris-HCl pH 8.1, 400 mM KCl, 5% (v/v) glycerol, 1 mM β-mercaptoethanol (BME), 0.5 mM PMSF, 30 mM imidazole). The resuspended cells were treated with 1mg of lysozyme per mL and incubated with stirring for 30 minutes. The cells were then treated with 2.5 mg/mL deoxycholic acid (Biobasic). Following a

further 30-minute incubation, the cells were lysed by sonication using a Branson Ultrasonic Corp sonifier with settings of 60% amplitude, 10 cycles, and 1 minute/cycle. The cell lysate was clarified by centrifugation for 30 minutes at 30 000 × *g* at 4 °C in a Sorval Lynx 6000 centrifuge (ThermoFisher) with a Fiberlite F14-14x50cy rotor, and the resulting supernatant was applied to 6 mL of Ni^{2+} Sepharose resin (GE health sciences) and incubated for 60 minutes at room temperature.

The resin was collected by centrifugation at 500 × *g* for 5 min, and the supernatant was replaced with five resin volumes of fresh Ni^{2+} buffer A to wash. The wash procedure was repeated four times, after which the resin was incubated with one resin volume of Ni^{2+} buffer B (20 mM Tris-HCl pH 8.1, 400 mM KCl, 5% (v/v) glycerol, 1 mM β-mercaptoethanol (BME), 0.5 mM PMSF, 200 mM imidazole) for 5 minutes to elute. The resin was then collected as above, and the supernatant was extracted. The elution procedure was repeated six times, with 50 μL of each elution reserved for SDS-PAGE analysis. The elutions were pooled and re-buffered by adding five volumes of Protein Storage Buffer (20 mM HEPES-KOH pH 7.5, 150 mM KCl, 1 mM BME, 0.5 mM EDTA, 5 mM $MgCl_2$, 20% (v/v) glycerol). This solution was concentrated 5-fold on an Amicon 10 000 Da MWCO spin column. This re-buffering was repeated twice, followed by further concentration of the solution to 5.91 mg/mL as determined by absorbance at 280 nm and a theoretical extinction coefficient of 83,310 M^{-1} cm^{-1} and stored at −80 °C.

3.6 Expression of pre-ribosomal complexes in *S. cerevisiae*

In preparation for the expression of pre-ribosomal particles from yeast, the appropriate strains (YDU1-central-5′Tob or YDU1-major-5′Tob) were cultured on SC-His-Leu agar plates with 2% glucose prepared using YNB + nitrogen and SC-His-Leu dropout mix supplement (Sunrise Science Products). Pre-cultures of 50 to 300 mL SC-His-Leu containing 2% raffinose (BioBasic) were grown at 30 °C overnight with shaking. The density of the precultures was recorded using a UV5nano spectrophotometer (Mettler Toledo) and used to inoculate 6 L of

medium to an OD_{600} of 0.2 unless otherwise stated in Table 3. Medium for the expression was SC-His-Leu containing 1.66 μg/mL doxycycline and 2% galactose or Yeast-peptone-galactose (YPG) medium containing 1.66 μg/mL doxycycline (2% peptone, 1% yeast extract, 2% galactose). Expression flasks were inoculated to an OD_{600} of approximately 0.2 and allowed to grow until an OD_{600} between 0.9 and 1.1 was reached. Once this optical density was reached, the cells were harvested by centrifugation at 5000 × *g* for 30 minutes at 4 °C in a Sorval Lynx 6000 centrifuge (Thermo Fisher) with a Fiberlite F9 6x1000 rotor. Cell pellets were washed in cold distilled deionized water (d_2H_2O), combined into a single tube, and pelleted again at 5000 × *g* for 5 minutes on a multifuge x3r centrifuge (Thermo Fisher) with a bioshield 1000A rotor before being shock frozen in liquid nitrogen and stored at −80 °C.

Conditions for the expression of pre-ribosomal complexes varied slightly from the basic protocol over the course of the multiple expressions. Deviations from the standard protocol are listed for each purification in Table 3.

3.6.1 Resin preparation for tandem purification

In preparation for the purification of pre-ribosomal particles, resins were coupled to appropriate ligands and washed at 4 °C or on ice. The composition of maltose and tobramycin wash buffers varied for each purification, as seen in Table 4. Dextrin sepharose resin (GE Healthcare) was washed three times by incubating with five resin volumes of maltose wash buffer, which was removed after collecting the resin at 500 × *g* for 5 minutes. After washing, the resin was adjusted to a 50% slurry and incubated with 7 μg of HMM protein per mL of resin for at least 4 hours. After incubation, the resin was washed an additional three times and stored as a 50% slurry.

Table 4: List of discussed purifications, including details of buffer conditions. Changes from one purification to the next are indicated in bold.

Purification	Strain	Expression Media	Maltose Wash Buffer	Tobramycin Wash Buffer	Resin Volume
2	YDU1-central-5′Tob	SC-His-Leu + 1.66 µg/mL (2 L)	100 mM HEPES, pH 7.9 200 mM KCl 1 mM EDTA 1 mM DTT 10 mM βME 10% glycerol 0.02% NP-40	20 mM HEPES, pH 7.9 2 mM $MgCl_2$ 150 mM NaCl 0.5 mM DTT 10% glycerol	1 mL
5	YDU1-central-5′Tob	SC-His-Leu + 1.66 µg/mL **(6 L)**	100 mM HEPES, pH 7.9 200 mM KCl 1 mM EDTA 1 mM DTT 10 mM βME 10% glycerol 0.02% NP-40	**100 mM HEPES, pH 7.9** **200 mM KCl** **2 mM $MgCl_2$** **1 mM EDTA** **1 mM DTT** **10 mM βME** 10% glycerol	1 mL
6	YDU1-central-5′Tob	SC-His-Leu + 4 µM doxycycline (1.66 µg/mL) (6 L)	100 mM HEPES, pH 7.9 200 mM KCl 1 mM EDTA 1 mM DTT 10 mM βME 10% glycerol **0.02% NP-40***	100 mM HEPES, pH 7.9 200 mM KCl 2 mM $MgCl_2$ 1 mM EDTA 1 mM DTT 10 mM βME 10% glycerol	1 mL
10	YDU1-Major-5′Tob	**YPG + 10 µg/mL doxycycline** (6 L)	100 mM HEPES, pH 7.9 200 mM KCl 2 mM $MgCl_2$ 1 mM EDTA 1 mM DTT 10 mM βME **20% glycerol** 0.02% NP-40	100 mM HEPES, pH 7.9 200 mM KCl 2 mM $MgCl_2$ 1 mM EDTA 1 mM DTT 10 mM βME **20% glycerol**	1 mL
11	YDU1-central-5′Tob	YPG + 10 µg/mL doxycycline (6 L)	100 mM HEPES, pH 7.9 200 mM KCl 2 mM $MgCl_2$ 1 mM EDTA 1 mM DTT 10 mM βME 20% glycerol 0.02% NP-40	100 mM HEPES, pH 7.9 200 mM KCl 2 mM $MgCl_2$ 1 mM EDTA 1 mM DTT 10 mM βME 20% glycerol	**2 mL**

*NP-40 is not present in the final 25% of washes for purification 6

Affigel-10 (Biorad) was removed from −80 °C storage and allowed to warm to 4 °C. The resin was washed three times by incubating with five resin volumes of tobramycin wash buffer, which was removed after collecting the resin at 500 × *g* for 5 minutes. The resin was then adjusted to a 50% slurry by the addition of one resin volume of 100 mM tobramycin (Biobasic) in 20 mM HEPES, pH 7.9. The resin was incubated with tobramycin for a minimum of 4 hours before the solution was supplemented with ethanolamine to a final concentration of 100 mM to block unreacted sites. Blocking took place over 1 hour, after which the resin was washed four times in wash buffer. The coupled resin was stored at 4 °C until use.

3.6.2 Tandem purification of pre-ribosomal complexes

Yeast cell pellets between 4 and 8 grams were suspended in 10 mL of maltose wash buffer supplemented with 10 μL Ribolock RNase inhibitor (Thermo Fisher) and 20 μL fungal protease inhibitor cocktail (Thermo Fisher). Cells were lysed six times at 11000 psi in a French pressure cell press. The lysate was clarified at 20 000 × *g* for 30 minutes in a Sorval Lynx 6000 centrifuge (Thermo Fisher) with a Fiberlite F14-14x50cy rotor and applied to 1 mL HMM bound dextrin sepharose resin unless otherwise stated in Table 4. Resin and clarified lysate were incubated with rotation at 60 RPM for 1 hour at 4 °C. The bound resin was placed in a disposable chromatography 10- or 2-mL column (as appropriate for the resin volume in Table 3) inside a conical centrifuge tube. The tube and column were centrifuged at <150 × *g* to increase the flow rate compared to gravity flow. The resin was washed with 20 resin volumes of maltose wash buffer. Washes were pooled in increments of 5 mL. Where indicated with an asterisk in Table 4, the resin was washed with 15 resin volumes of maltose wash buffer followed by five resin volumes of NP-40 free maltose wash buffer. Pre-ribosomal complexes were eluted with 1.5 mL of maltose elution buffer. In all cases, the maltose elution buffer consisted of a maltose wash buffer lacking NP-40 and supplemented with 10 mM maltose. Elutions were repeated to a total

of six resin volumes. For washes, 1 mL was reserved for later analysis. For each elution, 200 μL was reserved for subsequent analysis.

Elutions of pre-ribosomal complexes were pooled and applied to the tobramycin-coupled affigel-10 resin. The resin was incubated for 1 hour before being applied to a new 2- or 10-mL chromatography column within a conical centrifuge tube. The tube and column were centrifuged as above and washed with 20 resin volumes of tobramycin wash buffer. The snR30 was eluted with six resin volumes of tobramycin elution buffer (tobramycin wash buffer + 10 mM tobramycin) and collected in 1.5 mL increments.

Absorbances at 260 and 280 nm were recorded of all samples using a UV5nano spectrophotometer (Mettler Toledo). For select purifications, elution fractions were reserved at 4 °C for same-day negative stain grid preparation, and the remainder of the samples were shock-frozen in liquid nitrogen and stored at −80 °C.

3.7 Grid preparation for negative stain microscopy

Formvar Carbon grids (Electron Microscopy Sciences) were cleaned by plasma discharge for 15 seconds. 5 μL of the sample was applied to the grid and incubated at room temperature for 5 minutes. The excess sample was wicked away using filter paper, and the grid was washed three times by gentle immersion into distilled deionized water followed by wicking of excess liquid. The grid was then immersed into 2% uranyl acetate (Electron Microscopy Sciences) before the excess was wicked away. Negative stain imaging was performed at the University of Manitoba by Dr. Zev Ripstein and Timothy Vos

3.8 RT-PCR analysis

For each fraction to be analyzed by RT-PCR, the sample was combined with primer to a final concentration of 6 mM to create the annealing mixture. These primers are Tob tag antisense for snR30, 4xMS2 XhoI antisense for rRNA truncations, U14 RTPCR antisense for U14, snR10

RTPCR antisense for snR10, and 7SL Antisense for 7SL (Table 2). The sample and primer were denatured at 70º C and allowed to anneal at 4º C before the addition of 2 s of AMV reverse transcriptase with 2x RT buffer (NEB) and 500 μM dNTPs to create the reverse transcription (RT) mixture. The reaction occurred for one hour at 42º C. The initial sample comprised 50% (v/v) of the RT mixture.

PCR reactions for each sample were conducted in 1x PCR reaction buffer (NEB). The PCR reaction mixture was supplemented to a final concentration of 2.5% DMSO, 200 μM dNTPs, 1 unit of Taq polymerase, and 0.5 μM of each of the two primers and contained 10% (v/v) RT mixture as a template. For each reaction, the reverse primer used was the same as the RT reaction, and the forward primers were snR30-RTPCR-sense for snR30, rRNA-central RTPCR-sense for the rRNA central domain truncation, rRNA-major-RTPCR-sense for the rRNA major domain truncation, U14 RTPCR sense for U14, snR10 RTPCR sense for snR10, and 7SL sense for 7SL (Table 2). The PCR reactions were denatured at 98º C for 30 seconds, followed by 21−30 cycles of 95 °C for 10 seconds, 56 °C for 30 seconds, and 68 °C for 30 seconds. The final extension at 68 °C was conducted for an additional 2 minutes. The cycle number was reduced for certain purifications to generate a semi-dynamic detection range as opposed to amplifying to saturation.

RT-PCR reactions were analyzed either by 2% agarose gel developed for 35 minutes at 100 V and stained with Sybrsafe or 8% DNA PAGE developed at 120 V for 40 minutes and stained with Ethidium-bromide.

Chapter 4: Results

4.1 Assembly of plasmids for affinity-tagged RNAs

In order to perform a purification of snR30 bound, co-transcriptional ribosome precursors from yeast, it is first necessary to construct a strain capable of expressing functional snR30 with an RNA aptamer and a truncation of the rRNA containing a second RNA aptamer. Such a system allows for the expression and *in vivo* assembly of pre-ribosomes that is halted by the truncation of the rRNA precursor. These precursors then contain the MS2 aptamer, as well as a tobramycin binding aptamer while complexed with snR30 (Figure 3 A). This allows for the initial purification of pre-ribosomes based on the binding of MS2 protein to the MS2 aptamer (Figure 3 B), followed by selective separation of snR30 bound pre-ribosomes by tobramycin affinity chromatography (Figure 3 C).

To this end, I constructed a plasmid for the constitutive expression of snR30 containing a tobramycin binding aptamer in place of the loop on its 5′ hairpin, nucleotides 235-239 of the RNA. The tobramycin aptamer is a short RNA structure that binds the tobramycin antibiotic with high specificity and affinity [60]. This allows for purification without the usage of large protein intermediates [57]. The endogenous promoter and terminator of *snR30* are included to allow constitutive expression of the RNA. The encoded RNA is denoted as *snR30-5'Tob,* indicating that the tobramycin binding aptamer is inserted into the 5′ hairpin. I generated the *snR30-5'Tob* construct by insertional mutagenesis with primers containing a 5′-extension encoding the tobramycin binding aptamer (see Materials and Methods). After the mutation of the *snR30* gene within a pUC19 plasmid backbone, the resulting *snR30-5'Tob* gene was amplified by PCR and inserted into the SmaI site of a pRS313 shuttle vector for transformation into yeast cells, and Sanger sequencing confirmed that the gene was successfully inserted. This procedure was repeated with a wild type *snR30* to generate a pRS313-snR30 control plasmid expressing wild type snR30.

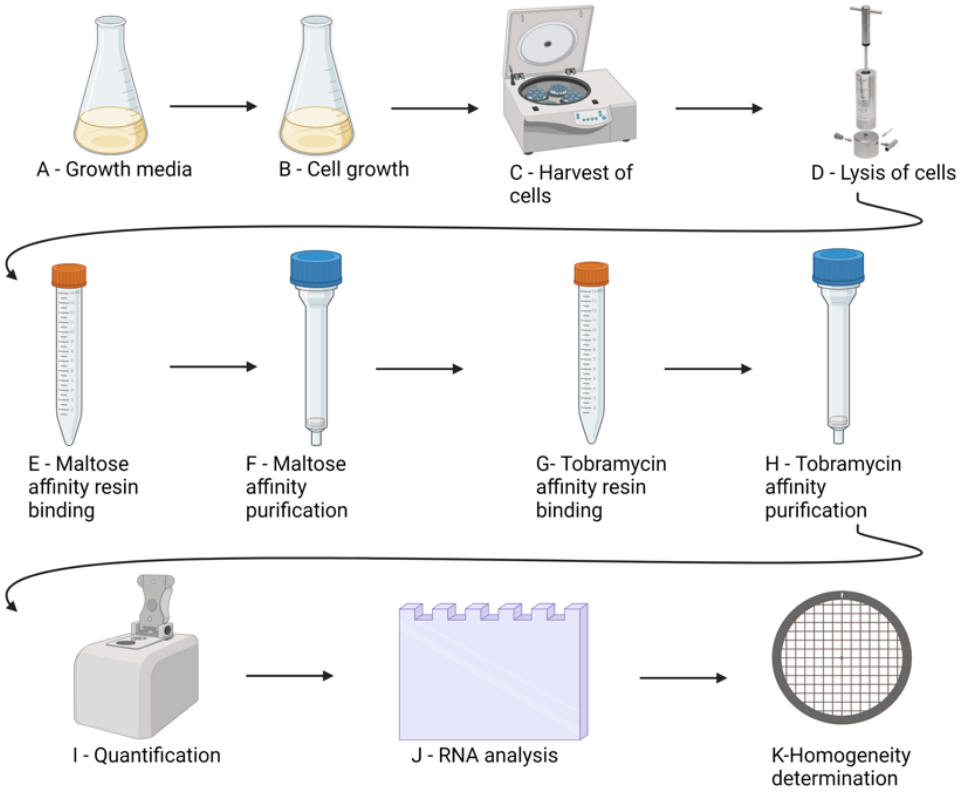

Figure 3Figure 3: Outline of workflow for the expression, purification, and analysis of snR30-bound pre-ribosomes from yeast.
Shown are the schematic representations of the steps of selection of the growth media for cells (**A**), the growth of the cells (**B**), the harvesting of the cells by centrifugation (**C**), and the lysis of the cells by high-pressure cell disruption (**D**). The purification of the resulting lysate is accomplished by binding it to a maltose affinity resin (**E**) and the subsequent washing and elution of pre-ribosomes from that resin (**F**). The elution fractions are then bound to a tobramycin resin (**G**), which is washed and eluted (**H**). Analysis of the purifications consists of spectrophotometry of the samples (**I**) followed by RNA detection through RT-PCR and gel analysis (**J**). For select samples, homogeneity and size were determined through negative stain electron microscopy (**K**).

To assess the function of snR30-5′Tob compared to snR30 wild type, the ability of snR30-5′Tob to complement the repression of snR30 in *S. cerevisiae* was tested. To accomplish this, the pRS313-snR30 and the pRS313-snR30-5′Tob plasmid were transformed into *S. cerevisiae*

strain YDU1, which contains *snR30* genomic copy under the control of a tetracycline/doxycycline repressible promoter. After the transformation of YDU1 with each plasmid, the resulting strains were grown on YPD-agar plates containing 2 μM doxycycline. YDU1 shows reduced growth on this medium due to the repression of the essential snR30 but the same conditions allow for the growth of YDU1 with snR30 complementation via pRS313-snR30 (Figure 4). The two replicates of the strain of YDU1-snR30-5′Tob are seen to grow on the same plate to a similar extent to YDU1-snR30 indicating successful complementation by the mutant snR30. This indicates that there is a successful incorporation of tagged snR30, which will allow for the purification of snR30-containing complexes via the tobramycin aptamer.

4.2 Transformation of the dual expression system

In order to prepare strains for the expression of pre-ribosomes containing tagged rRNA truncations and tagged snR30, I utilized previously prepared strains of YDU1 transformed with either pESC-Leu-Central or pESC-Leu-Major. These plasmids express tagged rRNA under the control of the Gal promoter, which is active in the presence of galactose and the absence of glucose (Table 3). The pESC-Leu-Central plasmid contains the first 1837 nucleotides of the RDN37-1 locus, followed by four repeats of the MS2 binding aptamer [61]. This aptamer binds the coat protein of the MS2 bacteriophage, and a 4x repeat has been used in previous studies with great success to purify pre-ribosomes [28, 40]. The truncated pre-rRNA gene is inserted between the SalI and XhoI sites of the pESC-Leu backbone. The pESC-Leu-Major is truncated from the same template, containing the first 2330 nucleotides of the RDN37 locus. These two truncations (central and major) were selected based on the ends of the domains of the 18S rRNA. These domains have distinct sets of proteins associated with them and form specific sections of the SSU precursor [37]. The precursor truncated to the central domain will form a pre-ribosome containing snR30 and the “body” of the SSU. The precursor truncated to the major domain will contain the first section of the “head” of the pre-ribosome in addition to the

components found in the previous construct. Following the transformation of both YDU1-Central and YDU1-Major with pRS313-snR30-5′Tob, the resulting strains grew successfully on selective media lacking both histidine and leucine, indicating the presence of both the pRS313 and pESC-Leu derived plasmid respectively.

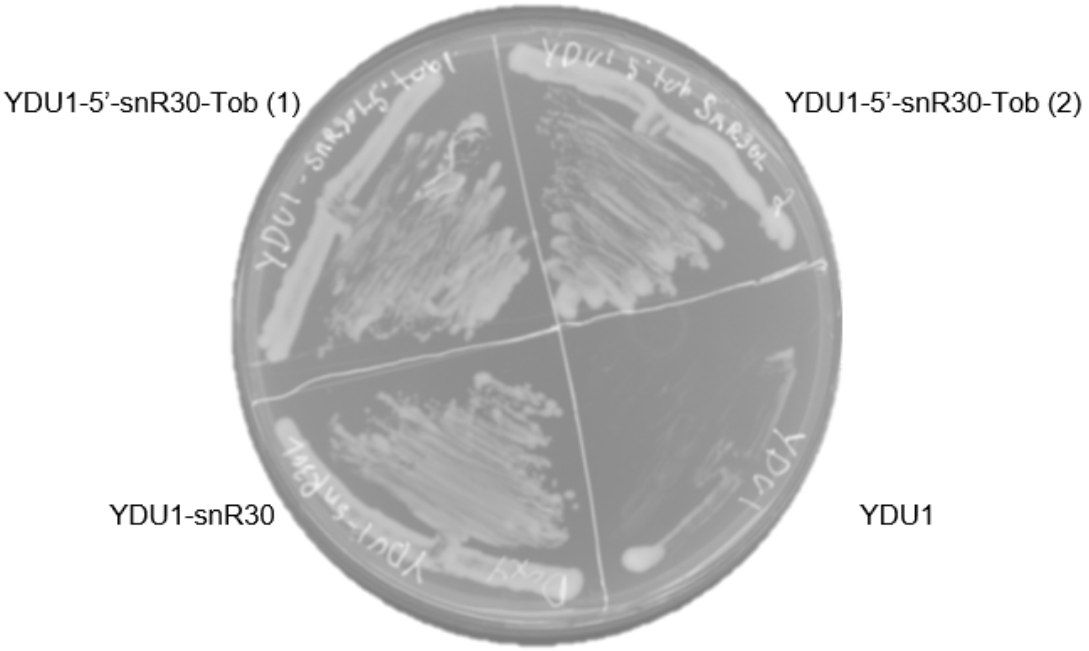

Figure 4: Growth complementation of snR30-repressed yeast strains by plasmid-derived snR30.
S. cerevisiae YDU1 with the snR30 gene under the control of a tetracycline/doxycycline-repressible promoter was grown on a YPD agar plate containing 2 µM doxycycline. Strains contained various plasmids to express snR30 variants under the native promoter, as indicated. Plates were imaged after growth for 2.5 days at 30 °C. Streaks of two individual colonies of YDU1-snR30-5′Tob, which expresses the tobramycin aptamer containing variant of snR30 via a pRS313-derived plasmid, are compared to complementation by pRS319-snR30 (positive control) and to YDU1 without rescue plasmid (negative control)

4.3 Purification of the snR30-associated pre-ribosome

I performed the purification of snR30-associated precursors based on published methods for the purification of pre-ribosomes using the MS2 aptamer containing pre-rRNA truncations [28, 40]. This purification utilizes the affinity of the MS2 aptamers for the MS2 coat protein. For the purification, I am using the Hexahistidine Maltose MS2 (HMM) protein which is a construct

designed for purifications of RNAs containing the MS2 aptamer. It is a fusion of the MS2 coat protein with a maltose binding domain and a 6× histidine tag. The maltose binding domain of the HMM protein has a high affinity for the dextrin groups allowing it to be immobilized onto a dextrin sepharose resin. The association of the HMM protein with the dextrin resin allows for the immobilization of complexes containing the MS2 aptamer via its interaction to the immobilized MS2 coat protein domain of HMM. The introduction of maltose to this system competes for the binding of the maltose binding domain and releases the HMM protein along with the bound RNA (Figure 5 A). While the hexahistidine tag of the HMM protein would have allowed for an alternative purification using nickel-sepharose chromatography, maltose affinity chromatography was preferable as the maltose eluent was predicted to be less disruptive to the pre-ribosome than the imidazole eluent utilized in nickel sepharose chromatography. Due to the chemical similarity between imidazole and histidine, imidazole has the potential to disrupt histidine dependent inter- and intra-protein interactions. To prepare for the pre-ribosome purifications, I used the hexahistidine tag to purify HMM after overexpression in *E. coli*.

Following the maltose affinity purification, I utilize the tobramycin-aptamer tagged snR30 to further purify those pre-ribosomes that contain snR30. This is accomplished utilizing a tobramycin derivatized resin. Affigel-10 resin forms a stable crosslink to primary amines under basic conditions. By incubating Affigel-10 with a high concentration of tobramycin, a tobramycin affinity resin is produced that will bind to RNAs containing the tobramycin aptamer. Addition of tobramycin to the system will elute the bound RNA by competing for the binding of the tobramycin aptamer (Figure 5 B).

The complete purification pipeline is outlined in Figure 3, and the major changes to specific steps are summarized in Table 3. In brief, *S. cerevisiae* cells were grown in liquid medium containing doxycycline for the repression of wild type snR30 and galactose for the transcription of the truncated rRNA (Figure 3 A, B). The cells were harvested by centrifugation and lysed

using a high-pressure cell disruptor (Figure 3 C, D). The lysate was then clarified and bound to the maltose affinity resin (Figure 3 E). The resin was washed in a wash buffer to remove cellular contaminants and eluted in a maltose-containing elution buffer (Figure 3 F).

The pooled elution fractions of the maltose affinity purification were bound to tobramycin derivatized affigel-10 (Figure 3 G) and washed to remove non-snR30-associated particles. The snR30-pre-ribosomes were eluted using a tobramycin-containing buffer (Figure 3 H). Following the purification procedure, the stored fractions were analyzed in order to determine the success of the purification. The results were analyzed by a combination of spectrophotometry, wherein the absorbance of the fractions at 260 nm (A_{260}) was recorded. To account for the dilution and concentration that occurs at each step of the purification, the total absorbance is reported as the product of the A_{260} value and the total volume of a given fraction in millilitres. This value is referred to as total A_{260}. The total A_{260} of the final elution was assessed with criteria based on estimated minimum sample amounts required for mass spectrometry and cryo-electron microscopy, which must be greater than 0.05 and 0.2, respectively. Additionally, the fractions were analyzed by RT-PCR for the detection of the tagged RNAs. Detection of the tagged RNAs in the elutions of the purifications but not the late washes was taken as an indicator of successful binding to the resins.

The purifications saw several revisions in both the expression and purification procedures based on the results of preceding purifications. The procedure was altered to increase the stability of the particles following several purifications where the protein contents of the purification precipitated at step G (Figure 3) of the purification. These changes involved alterations to the buffer system utilized in steps E-H to prevent precipitation, as well as changes to resin preparation.

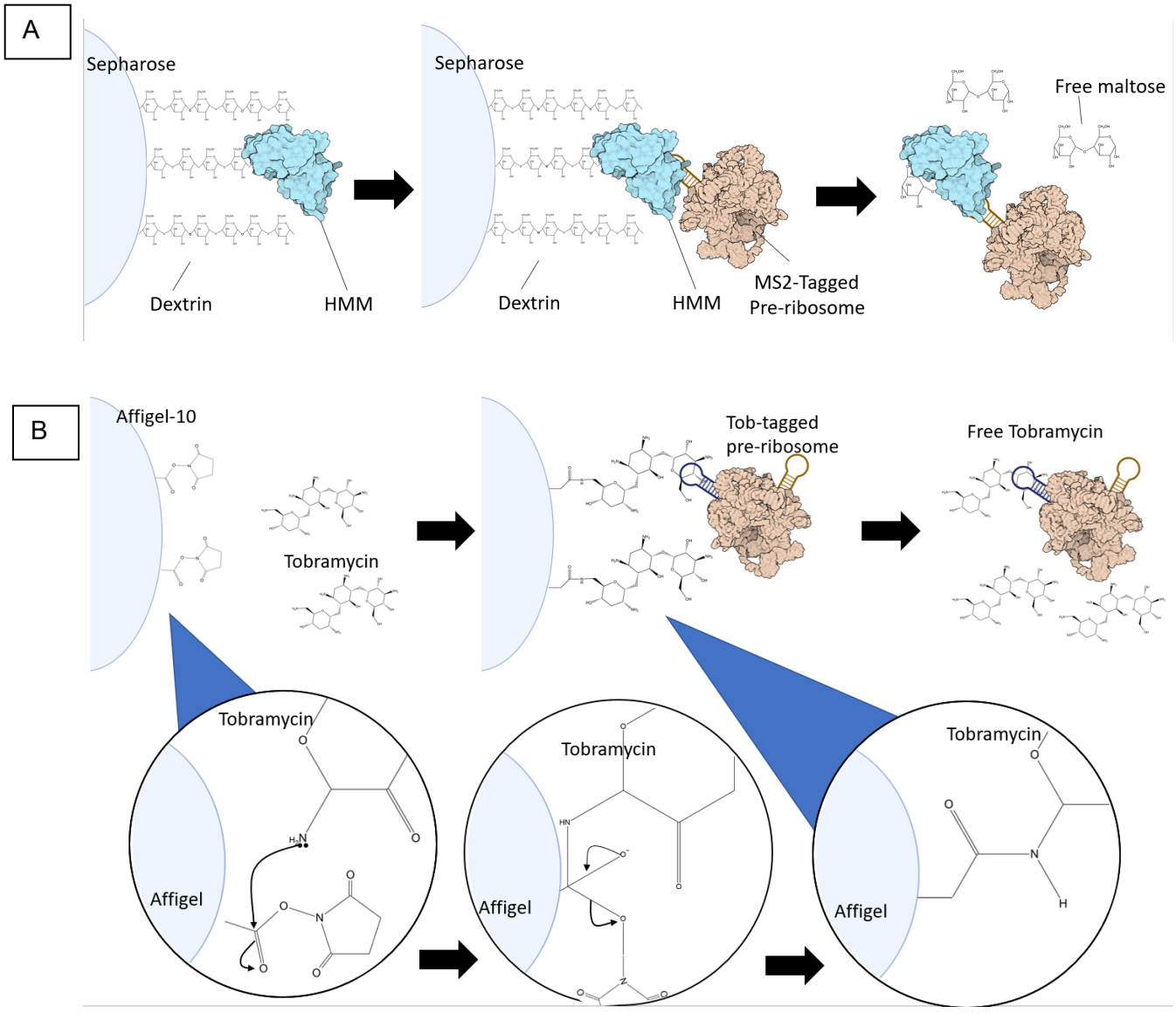

Figure 5: Schematic representation of the binding of the pre-ribosome to chromatography resins.

Shown are the schematic representations of the binding of the pre-ribosomes to the dextrin Sepharose resin (A) and the tobramycin resin (B). The dextrin Sepharose resin consists of dextrin units that bind the HMM protein. The MS2-tagged pre-ribosome binds the HMM protein and the pre-ribosome-HMM complex is eluted by the addition of free maltose. The Affigel 10 resin form a covalent bond to the primary amine of the tobramycin molecule under basic conditions. The tobramycin-tagged snR30 within the pre-ribosome binds the tobramycin derivatized Affigel-10 until eluted by the addition of free tobramycin. Representations of HMM and the pre-ribosome are adapted from PDB structures 1MPD and 6ZQB, respectively [18, 59].

Further changes aimed at increasing the amount of product obtained in step H of the purification and involved changes to the expression media and growth stage (Figure 3 A, B), changes in harvesting and lysis (Figure 3 C, D), and changes to the buffer conditions and resin volumes across both purifications (Figure 3 E-H).The most impactful changes and associated purifications are detailed in this thesis. The impactful changes are those that saw an improvement in the amount of product compared to previous purifications or saw an increase in the stability of the complexes, as seen in a lack of precipitation upon incubating with the tobramycin resin (Figure 3 G). For an exhaustive list of purifications, including failed purifications, see Appendix Table A1.

4.3.1 Purification 2

For the first notable purification of snR30-associated ribosomal precursors, I utilized a cell pellet of YDU1-central-5′Tob cells grown in 2 L of selective SC-His-Leu medium containing 1.33 µg/mL doxycycline. The cells were induced by the addition of galactose at the early log phase and allowed to grow to the late log phase. I utilized maltose affinity chromatography in a set of HEPES-based buffers based on published pre-ribosomal purifications to enrich the pre-ribosomes tagged with the MS2 aptamer [28] (Figure 3 E, F). I analyzed which fractions contained the target RNAs using DNA-PAGE of RT-PCR reactions. It is expected that tagged rRNA will result in a band near 430 bp when it is present. The gel shows no bands when the reaction targets the tagged pre-rRNA, except for a single band in the elution near 700 bp (Figure 6), indicating that there was no detectable presence of pre-rRNA in these samples. When analyzed for the presence of snR30, bands appear in the late wash and elution fractions (Figure 6). These bands are observed at approximately 250 bp and 90 bp, the largest of which corresponds to the expected size for the amplified fragment of snR30, which is 230 bp. The bands at 700 bp and 90 bp are attributable to mis-annealing of primers in a complex sample.

Only bands at the expected size can be taken as evidence for the presence of the targeted RNAs.

In order to further purify the snR30-containing pre-ribosomes from the elution fractions of the first purification, I utilized tobramycin-coupled affigel-10 resin. The elution fractions were bound to this resin, followed by wash and elution in buffers based on existing tobramycin affinity purifications of large RNPs in the literature [62] (Figure 3). Analysis of this purification using the same RT-PCRs yielded no bands when the rRNA precursor is targeted. The analysis shows two bands, one near 215 bp and one near 90 bp, in all fractions associated with the tobramycin affinity purification (Figure 6). Based on the expected size of 230 bp for the amplified fragment of snR30, a band corresponding to snR30 is, therefore, present in all stages of the tobramycin affinity purification.

Based on these results, it appears that a small amount of tagged snR30 is present across the purifications, being more concentrated in the later steps after the tobramycin affinity purification of tagged snR30. These results do not allow conclusions regarding the presence of the pre-rRNA across the purification, as the expected band is not seen in any purification.

4.3.2 Purification 5

Following the previous purification, several attempts were made to increase the amount of snR30-bound pre-ribosomes. The most drastic of these changes was a change to the harvesting of the cells (Figure 3 B). Cells were harvested at an OD_{600} of 1.0 as opposed to an OD_{600} greater than 3.0. Due to differences in the expression level of ribosome assembly factors, cells in early log phases were predicted to contain greater amounts of pre-ribosome per cell [63]. To account for the lower amount of cells per litre of culture when harvest at an earlier point, the cells were inoculated in 6 L of selective medium as opposed to 2 L. This media contained 2% galactose for the induction of the Gal promoter. To avoid contamination by glucose, which represses the Gal promoter, the cells were inoculated from a pre-culture using raffinose as a

carbon source. While this procedure increased the amount of pre-ribosomes purified, it resulted in frequent precipitation during the binding of the sample to the tobramycin affinity resin (Figure 3 G).

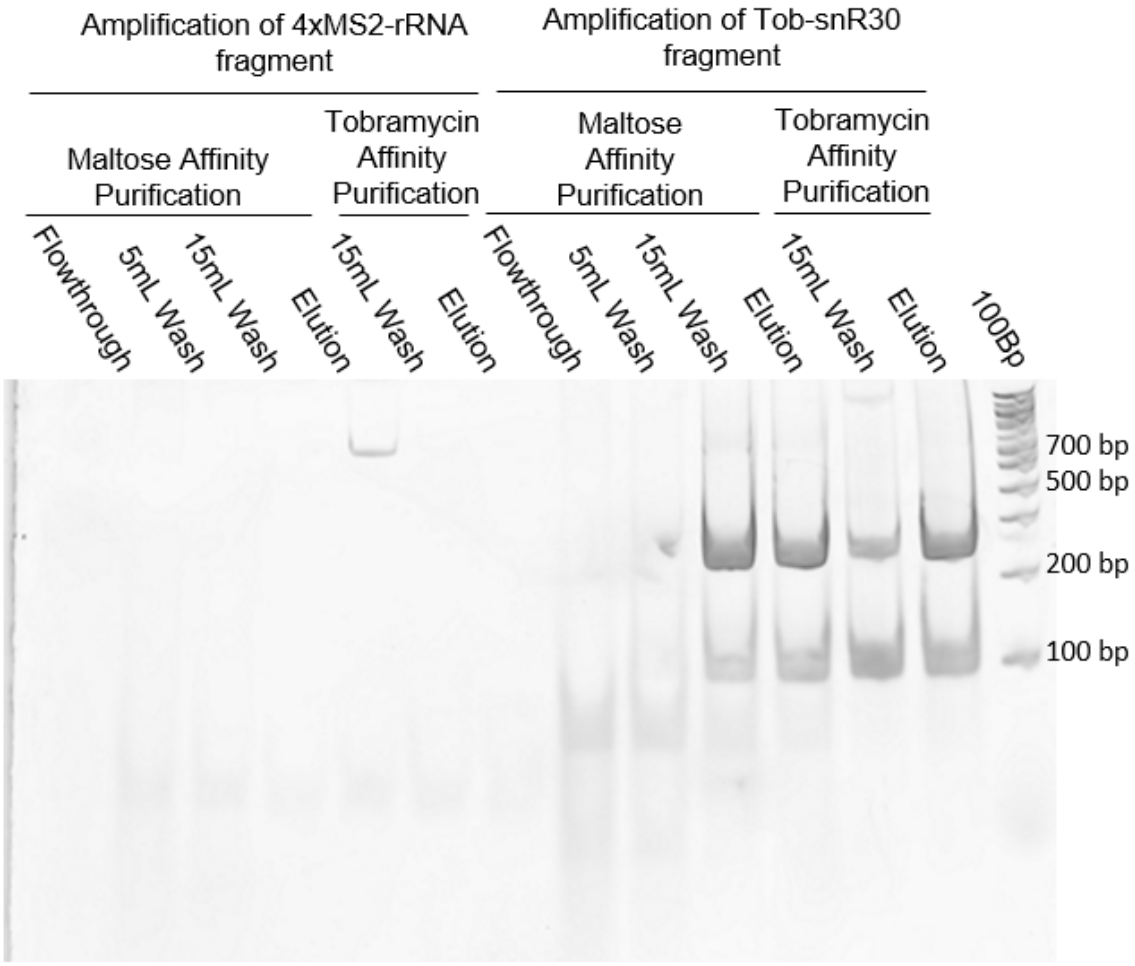

Figure 6: RT-PCR analysis of pre-ribosome purification 2.
Pre-ribosomes were first enriched by maltose affinity purification using MS2-tagged rRNA precursor truncated to the central domain, followed by tobramycin affinity purification of pre-ribosomes bound to tobramycin-aptamer tagged snR30. An Ethidium-bromide-stained 8% DNA-PAGE gel showing RT-PCR reactions targeting sections of the MS2-tagged rRNA precursor or the tobramycin-tagged snR30. For MS2-tagged rRNA, a band is expected at 430 bp. A band is expected at 215 bp for the tobramycin-tagged snR30.

This issue was addressed by altering the buffer system to a buffer with a higher buffering capacity and increased salt concentration (Table 2). In brief, this change consisted of the increase of HEPES from 20 mM to 100 mM and the substitution of 150 mM NaCl with 200 mM KCl, as well as the addition of 1 mM EDTA. This change in the buffer system results in a set of buffers for tobramycin affinity purifications that is more similar to the buffers utilized for the maltose affinity purification.

The analysis of the maltose affinity steps of purification 5 (Figure 3 E, F) by spectrophotometry (Figure 7 C) showed that there was a decrease in absorbance at 260 nm (A_{260}) across the washing steps of the purification, with an increase in the total absorbance in the elution compared to the late wash. This indicates the pre-rRNA was bound to the resin in a fashion that is released by the addition of the maltose elution buffer. The absorbance at 260 nm was also recorded for samples collected from the subsequent tobramycin affinity purification (figure 3 G, H). Absorbance in this purification is seen to decrease across the washing steps but to be high in the elution, indicating binding of snR30-5′Tob to the tobramycin resin that is subsequently eluted by the tobramycin elution buffer. The value of the total A_{260} in the final elution from the tobramycin column is greater than 0.2 indicating that this purification produced sufficient product for later analysis by cryo-EM and mass spectrometry.

I further analyzed the results of both stages of the purification process (Figure 3 E-H) by RT-PCR and agarose gel electrophoresis. RT-PCR of a fragment of the tagged rRNA precursor yields bands at 430 bp in the flow-through and elutions for the maltose affinity purification. Similar bands are present in the flow-through of the tobramycin affinity purification as well as the first elution from the tobramycin resin (Figure 3 G, H; Figure 6 A). When testing for the presence of the tobramycin-tagged snR30 primers by RT-PCR, bands at the expected size of 215 bp are observed in all fractions of the maltose affinity purification. The bands are also present in the

lanes corresponding to the flow-through, late wash, and first two elutions of the tobramycin affinity purification (Figure 7 B).

Based on the results of the RT-PCR and the accompanying absorbances, I conclude that the rRNA precursor and snR30 were both present across the purification and enriched in the final elution of the tobramycin affinity purification compared to the washes. I can further conclude that this purification produced sufficient amounts of particles for analysis by mass spectrometry and cryo-electron microscopy to be feasible.

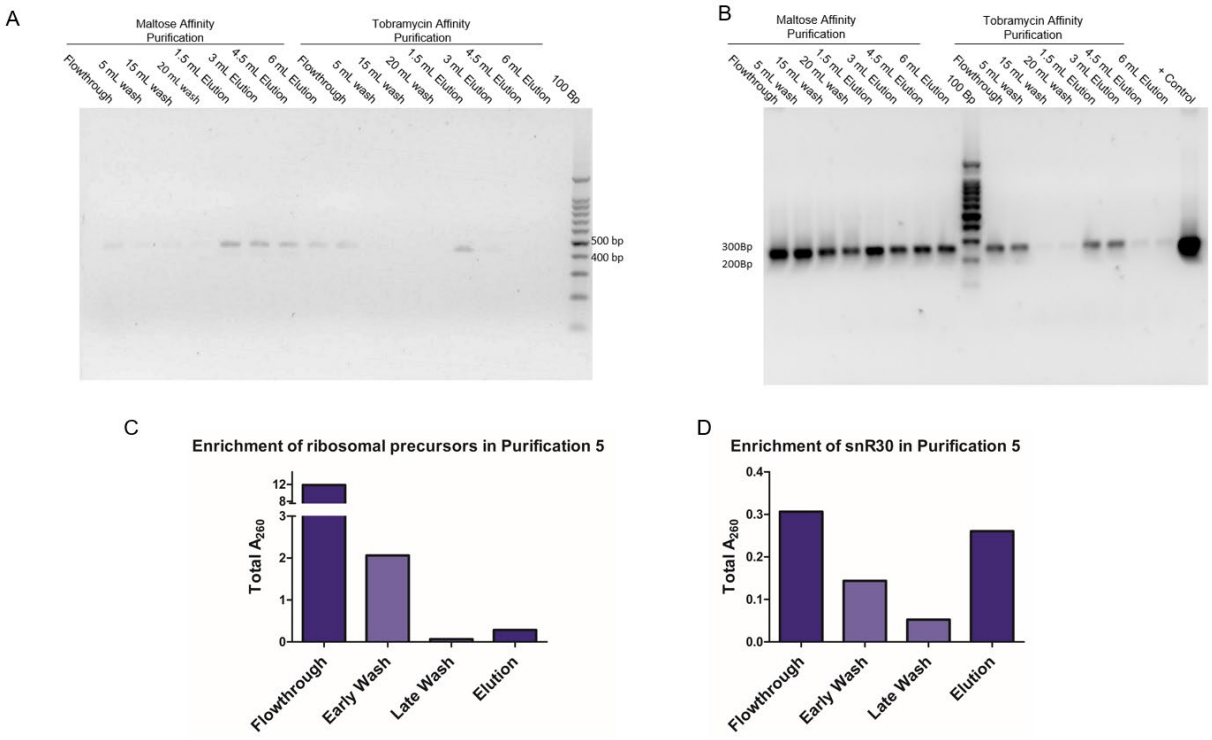

Figure 7: RT-PCR and absorbance analysis of pre-ribosome purification 5.
The purification of pre-ribosomes was adjusted to be from the lysate of early log phase cells harvested from 6 L of media. Pre-ribosomes were first enriched by maltose affinity purification using MS2-tagged rRNA precursor truncated to the central domain, followed by tobramycin affinity purification of pre-ribosomes bound to tobramycin-aptamer tagged snR30. Sybrsafe stained 2% agarose gels showing RT-PCR reactions targeting sections of the MS2-tagged rRNA precursor (**A**) or the tobramycin-tagged snR30 (**B**). A band is expected near 430 bp when primers for MS2-tagged rRNA are used. A band is expected near 215 bp when primers corresponding to tobramycin-tagged snR30 are used. The + control lane displays the PCR reaction of plasmid DNA containing the snR30L-5′Tob gene. The absorbance of individual fractions was also measured across both purifications and used to determine the total A_{260} for

each fraction. Total A_{260} is calculated as A_{260} multiplied by the volume (mL). Graphical representation of the total A_{260} of fractions from the purification of ribosomal precursors (**C**) and the further enrichment of snR30 (**D**). Total A_{260} for elutions represents the absorbance in the first elution fraction.

4.3.3 Purification 6

Following the success of purification 5, I performed another purification under similar conditions in order to generate more precursors for structural and compositional analysis. The expression and purification conditions remained identical with purification 5 except for the removal of the NP-40 detergent in the final 5 mL of washes with maltose wash buffer. The removal of buffer was intended to facilitate potential liquid chromatography-mass spectrometry analysis as the presence of detergent is potentially damaging to the liquid chromatography resin.

After performing spectrophotometry of the samples from the maltose affinity chromatography of purification 6 (Figure 3 E, F), I observed that the total absorbance of the early wash decreases only slightly compared to the flow-through. The late wash had a dramatically decreased total absorbance and was similar to the absorbance of the elution (Figure 8 B). The total absorbance of the elution of the maltose affinity purification is approximately half what was found in the maltose affinity steps of purification 5 (Figure 7 A). This indicates that this purification 6 resulted in less of the target complex being released at the elution step. My analysis of the tobramycin affinity purification shows a decrease in the total absorbance of the late wash compared to the early wash, with a small increase of the total absorbance at 260 nm in the elution relative to the final wash. While the absorbance of the elution is increased relative to the final wash, the amount is lower than that of the previous purification, indicating that the amount of product in this purification is an order of magnitude lower than the amount produced in purification 5 (Figures 4 C and 5 D).

Upon analyzing the purification using RT-PCR and agarose gel electrophoresis, I saw the expected bands at 430 bp, corresponding to the presence of the MS2-tagged rRNA precursor in the flowthrough and elution of the maltose affinity purification, as well as faintly in the elution of

the tobramycin affinity purification (Figure 8 C). Bands appeared at 215 bp in the elutions of both the maltose and tobramycin affinity purifications when the RT-PCR targeted the tobramycin-tagged snR30 and also appeared faintly in the late wash of the tobramycin affinity purification. Based on the spectrophotometry of these samples, it seems that the sixth purification had a lower yield in the tobramycin purification, despite the presence of RNA following the expected patterns in the RT-PCR analysis. Based on the total A_{260} of this final elution being less than 0.05 , neither LC-MS nor cryo-electron microscopy could be performed on this sample.

In order to determine the suitability of these complexes for structural analysis, I spotted the elution of the tobramycin affinity purification on a carbon grid and stained it with uranyl acetate. The grid was imaged on a Talos-TEM at 45 000× magnification. The resulting negative staining EM image contained several complexes that are approximately 20 nm in diameter, which is similar to the expected size for a nucleolar ribosome precursor (Figure 9 B) [53]. The particles themselves appear round or slightly oblong. While the particles appear as the expected monomer in some cases, three of the seven particles appear as a dimer instead. I could not perform an effective classification of 2D images, as the density of particles was not sufficient for averaging multiple particles (Figure 9 A).

4.3.4 Purification 10

Following several rounds of optimization of both the -central domain truncated rRNA construct and the -major domain truncated complex, I determined that despite reductions of precipitation introduced by changes to the buffer system, precipitation of proteins during binding of the sample to the tobramycin resin was a major factor inhibiting the success of the purifications. As well, the amount of product found in the final elution of the tobramycin affinity purification (Figure 3 H) remained too low for the target analyses of mass spectrometry and cryo-EM microscopy. In order to determine if the successful expression of tagged snR30 and its binding to the pre-ribosome was a limiting factor, the tenth purification consisted of cells of YDU1-major-

5′Tob grown in YPD medium containing 10 µg/mL doxycycline as opposed to the previous 1.66 µg/mL.

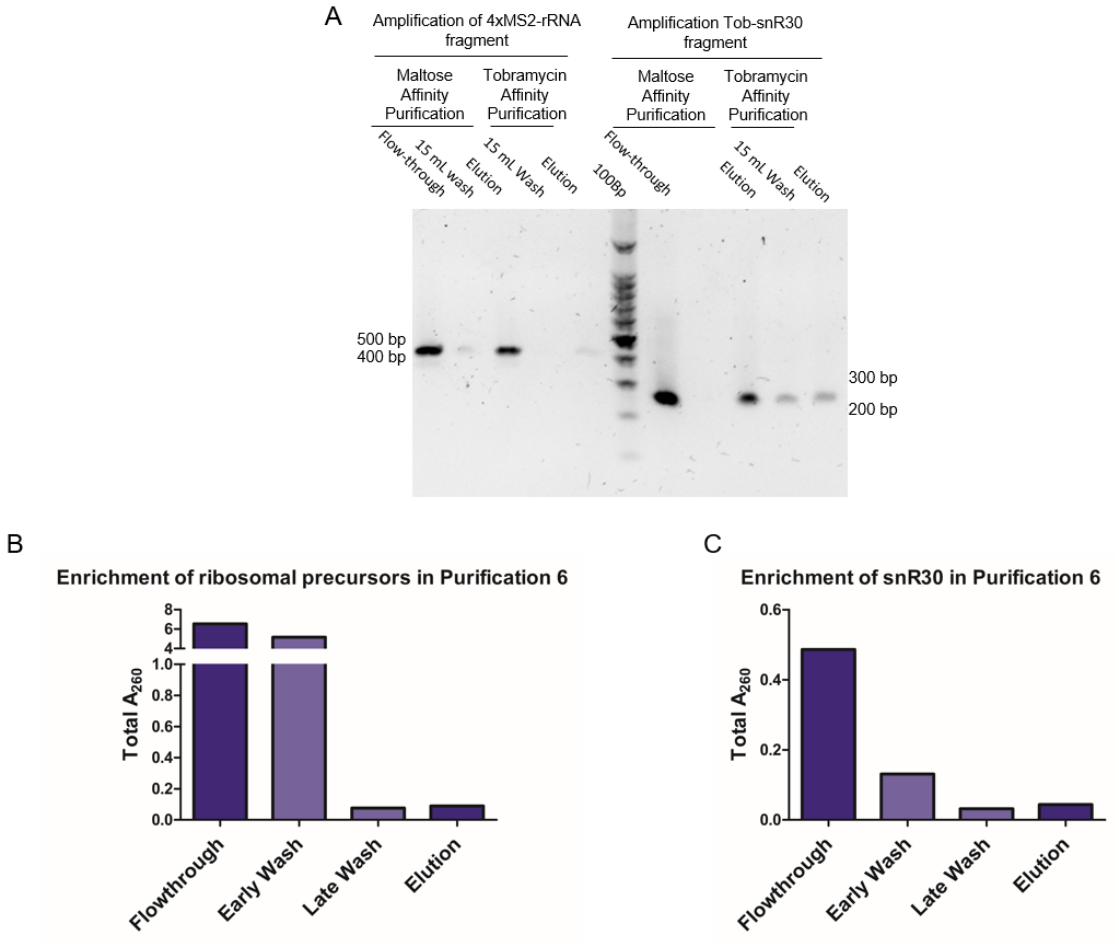

Figure 8: RT-PCR and absorbance analysis of pre-ribosome purification 6.
The prior purification was repeated for further analysis of the purified precursors. As in Figure 3, the pre-ribosome was enriched by tandem purifications, first targeting the MS2-aptamer on the rRNA truncation and then the tobramycin aptamer on snR30. RT-PCR was used to detect target RNAs in the purification with primers corresponding to sections of the MS2-tagged rRNA precursor or the tobramycin-tagged snR30. RT-PCR results are visualized on 2% agarose gels stained in Sybrsafe. For MS2-tagged rRNA, a band is expected at 430 bp. A band is expected at 215 bp for the tobramycin-tagged snR30 (**A**). Fractions of the same purification were also analyzed by spectrophotometry. Graphical representation of the total A_{260} of fractions from the purification of ribosomal precursors (**B**) and the further enrichment of snR30 (**C**). Total A_{260} for elutions represents the absorbance in the first elution fraction. Total A_{260} is calculated as A_{260} multiplied by the volume (mL).

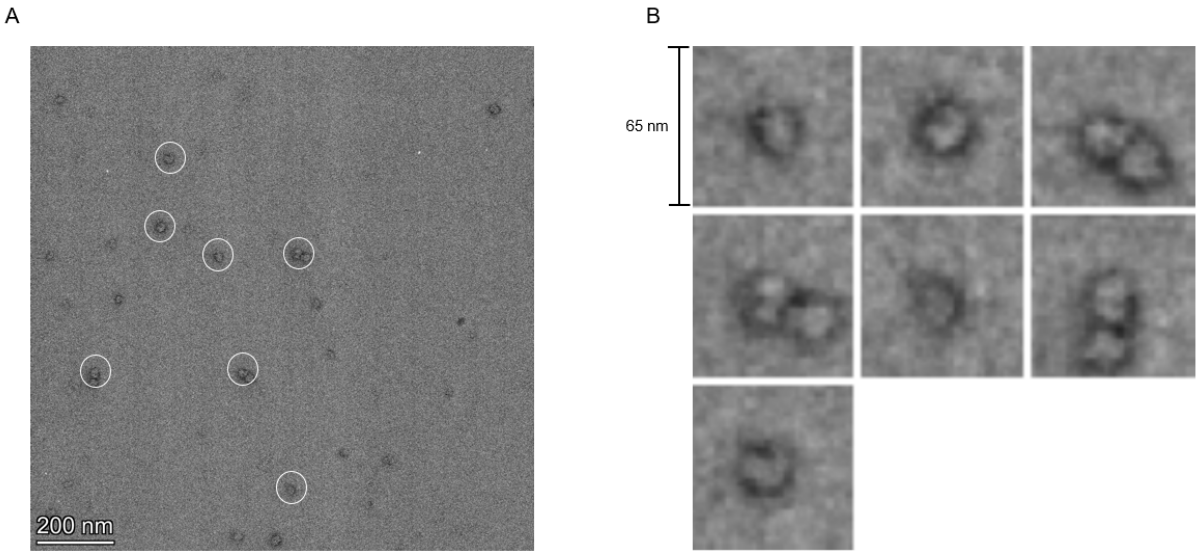

Figure 9: Electron micrograph of negative stained particles from pre-ribosome purification 6 Images were taken on a Talos Cryo-TEM with a Ceta 16M camera at 45 000× magnification. Particles highlighted in (**A**) are of the expected size for the ribosomal precursor and are shown individually in (**B**).

The doxycycline/tetracycline repressible promoter present in YDU1 represses snR30 transcription in a concentration dependent manner. An increase in doxycycline concentration was utilized to ensure that wild type snR30 was fully repressed. The cells expressing the major domain construct were tested as they accumulate a later stage of assembly that may be more stably bound to snR30. In order to further stabilized the constructs, I lysed these cells and purified the clarified lysate in a set of buffers with glycerol concentrations increased to 20% (v/v) from the previous 10% (v/v). The increase in glycerol concentrations was made in an attempt to prevent the precipitation of proteins during the purifications. Increasing the concentration of glycerol was predicted to stabilize the complexes by providing an environment that better mimicked the less polar and highly crowded nucleolus. Unlike previous purifications, the

spectrophotometry of the samples from this purification showed a decrease in absorbance across all steps, including the elutions, for both the maltose affinity and tobramycin affinity purifications (Figure 10 A, B). The total A_{260} of the elutions from both columns was below the 0.05 threshold for mass spectrometry analysis. Given the low total absorbances of the maltose and tobramycin affinity steps, there was a high amount of complex lost during both purifications. (Figure 10).

I subjected the fractions of this purification to RT-PCR analysis with the previously utilized primers targeting snR30-5′Tob and a new set of primers that are expected to result in a band at 230 bp if the MS2-tagged -major rRNA truncation is present (Figure 10 A, B). The RT-PCR analysis shows the expected bands in all fractions except for the late wash of tobramycin affinity purification. This indicates that both the tagged rRNA and the tagged snR30 are present throughout both the maltose affinity and tobramycin affinity purification.

The analysis of the total absorbance at 260 nm indicates that this 10th purification was unable to isolate sufficient amounts of pre-ribosomes for in-depth analysis. However, the enrichment of tagged RNAs in the elution of the tobramycin resin compared to late washes indicates that there is some binding of the complexes to the resins. These results together indicate that the optimizations failed to increase the amount of product but did prevent precipitation, as no precipitation was observed during the purification.

4.3.5 Purification 11

In order to achieve a higher yield of the target snR30-bound pre-ribosomes, I utilized a higher volume of both resins. Due to the finite binding capacity of each resin, an increase in the resin volume can provide the opportunity for more of the target RNA to bind in each case. The resin volumes for both the maltose affinity purification and the tobramycin purification were doubled to 2 mL.

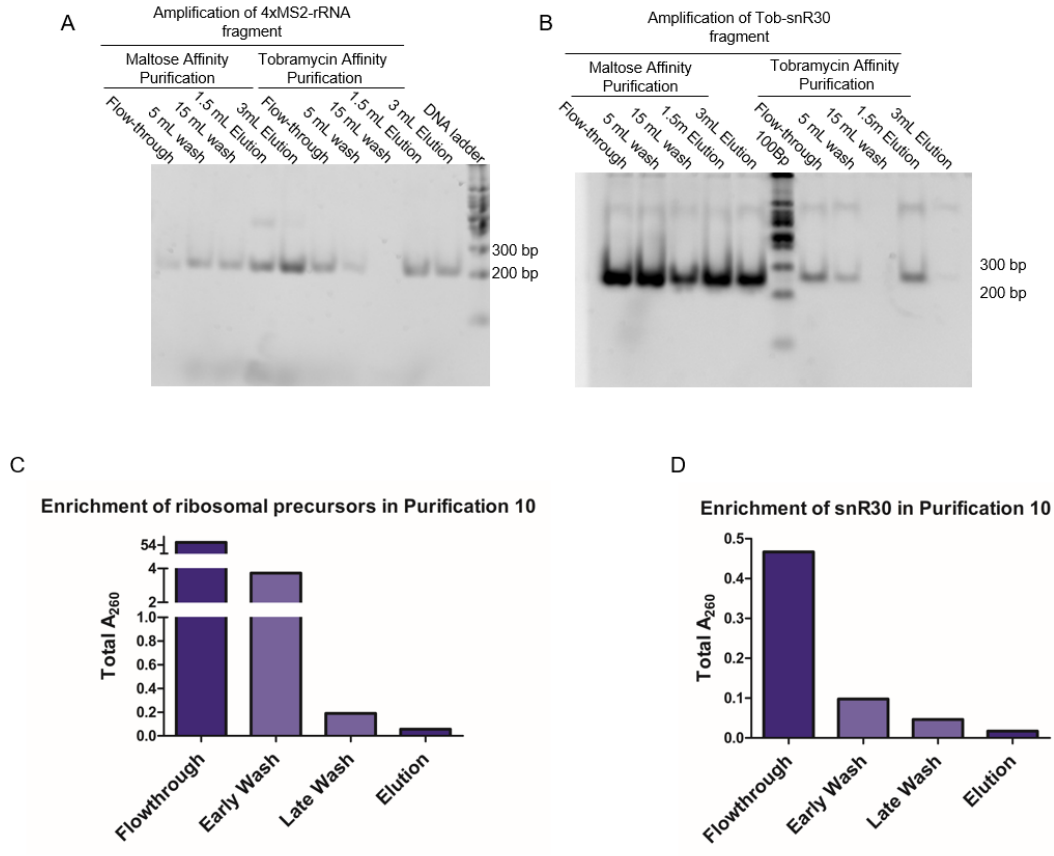

Figure 10: RT-PCR and absorbance analysis of pre-ribosome purification 10.
Pre-ribosomes produced by truncation to the 18S rRNA major domain were first enriched by maltose affinity purification using MS2-tagged rRNA (**A**), followed by tobramycin affinity purification of pre-ribosomes bound to tobramycin-aptamer tagged snR30 (**B**). Both purifications took place in buffers adjusted for improved complex stability. Ethidium-bromide-stained 8% PAGE gels showing RT-PCR reactions targeting sections of the MS2-tagged rRNA precursor or the tobramycin-tagged snR30. The primers amplify a region of approximately 230 bp for the MS2-tagged rRNA-central truncation and a region of approximately 215 bp for the tagged snR30 construct. The absorbances of the fractions were measured and are displayed graphically for the maltose affinity purification (**C**) and the enrichment by tobramycin affinity purification (**D**). Total A_{260} for elutions represents the absorbance in the first elution fraction. Total A_{260} is calculated as A_{260} multiplied by the volume (mL).

It was expected that the increase in resin volume would result in more complexes binding to the resin successfully, resulting in more pre-ribosomes present in the elution of both the maltose affinity step and the tobramycin affinity step (Figure 3 F, H). This purification utilized the same

high glycerol buffers as purification 10 (Table 3). The YDU1-central-5′Tob cells were utilized in this purification in order to make the purification more comparable to earlier purifications such as purification 5 and purification 6.

The spectrophotometry of this purification showed that in the maltose affinity purification, there is an increase in total A_{260} in the elution compared to the final wash (Figure 8 B). This indicates that the complex is being eluted upon the addition of elution buffer but remains bound in the presence of wash buffer (Figure 3 E, F). Furthermore, the total A_{260} is greater than 0.15. While this does not meet the criteria for structural analysis, it is closer to that value than previous purifications. The samples collected from the tobramycin affinity chromatography steps (Figure 3 G, H) do not show an increase in the elution relative to the late wash. The total absorbances of the fractions of the tobramycin affinity steadily decrease, indicating a lack of overall enrichment of the snR30-pre-ribosome complex in the final elution (Figure 11 C).

My RT-PCR analysis of this purification shows the predicted bands for the presence of MS2-tagged rRNA precursors across the washes and elution of the maltose affinity purification and in all stages of the tobramycin affinity purification except for the late wash. The snR30 targeting RT-PCR shows a different pattern with the expected 230 bp band appearing in the maltose affinity purification flowthrough, early wash, and elution but in no stages of the tobramycin purification. Based on the lack of snR30 detection and the absorbance of the second purification, I can conclude that this purification is characterized by limited binding of the complex to the tobramycin resin despite the increased resin volume.

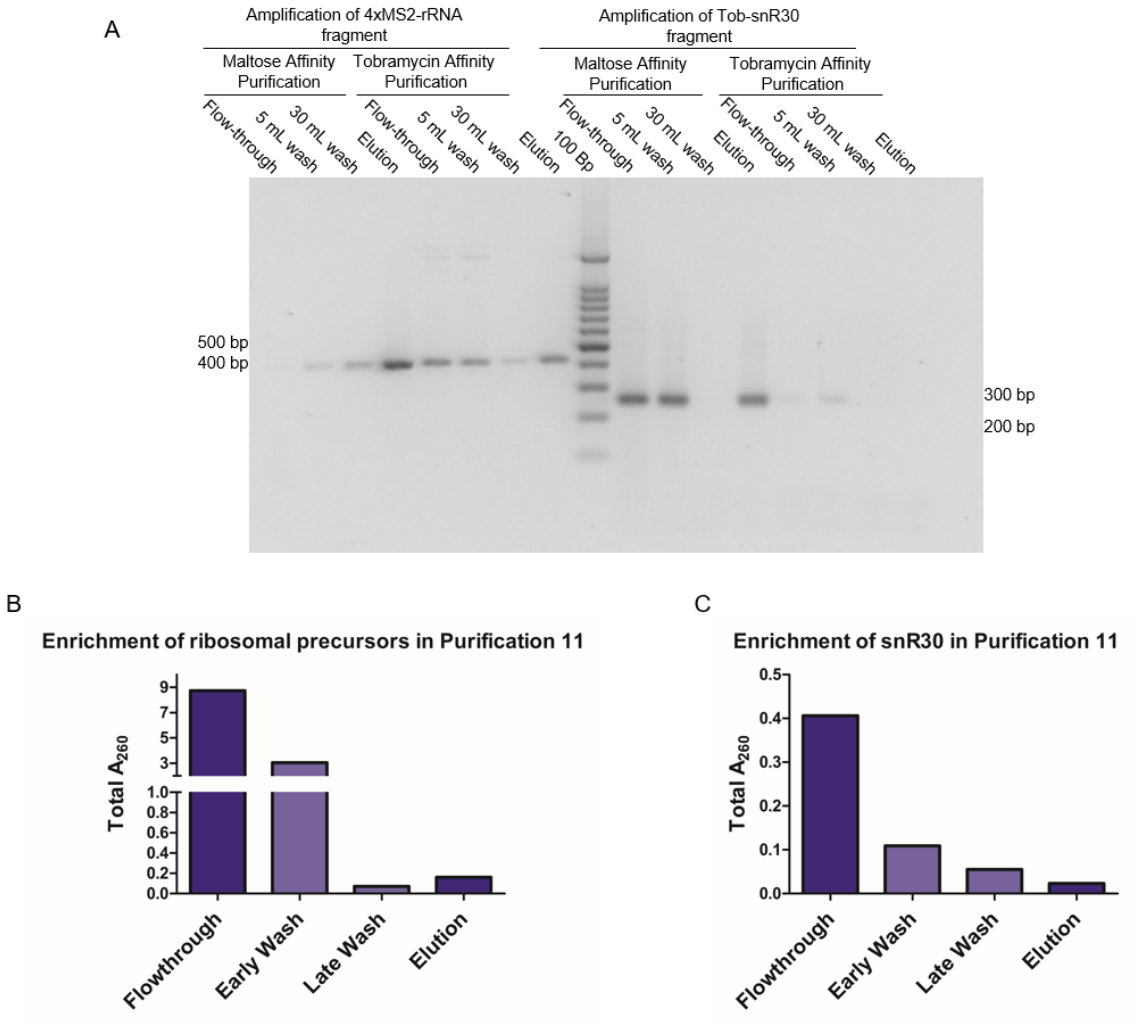

Figure 11: RT-PCR and absorbance analysis of pre-ribosome purification 11.
Enrichment of snR30-bound pre-ribosomes was achieved by tandem purification: Maltose binding chromatography was used to isolate pre-ribosomes based on the MS2 binding aptamer, followed by an enrichment of tobramycin binding aptamer tagged snR30. SybrSafe stained 2% Agarose gels showing RT-PCR reactions targeting sections of the MS2-tagged rRNA precursor or the tobramycin-tagged snR30. RT-PCR analysis targeting the MS2 aptamer tagged rRNA is expected to yield a 430 bp band if the RNA is present. For RT-PCR targeting the tobramycin-tagged snR30, a band of 215 bp will be generated if the RNA is present. Also shown is a graphical representation of the total A_{260} of fractions from the purification of ribosomal precursors (C) and the further enrichment of snR30 (D). Total A_{260} for elutions represents the absorbance in the first elution fraction. Total A_{260} is calculated as A_{260} multiplied by the volume (mL).

Chapter 5: Discussion

5.1 Creation of a dual-tagged system for the purification of snR30-bound pre-ribosomes

The goal of this project was the development and optimization of a system that allows for the purification of specific stages of the eukaryotic pre-ribosome in complex with the small nucleolar RNA, snR30. In order for this system to be deemed successful and effective, it must demonstrate the ability to selectively isolate a stable pre-ribosomal complex from *S. cerevisiae* that contains the expected components of the pre-ribosome at the target stage and snR30. The further goal of this project is to optimize the system such that it produces a sufficient amount of pre-ribosomal particles with a sufficient level of homogeneity for structural and biochemical investigation. This system would function as a novel way to analyze the mechanisms of snoRNAs during ribosome biogenesis. While single RNA aptamers have been utilized in combination with protein-based purification approaches, the usage of a dual aptamer system is entirely novel for the study of pre-ribosomes. RNA aptamer purifications in tandem have been previously utilized to study other RNP complexes; however the usage of aptamers located on two different RNAs within the same complex is novel compared to the established procedures of placing two aptamers on the same transcript [62]. This system is of particular interest for the study of the mechanism of the snoRNP due to the fact that it ensures the enrichment of snR30.

While I focussed here first on the direct purification using tagged snR30, it could be an interesting alternative to purify pre-ribosomes utilizing tagging of proteins associated with snR30. Given that the exact nature of the binding of snR30 to proteins during ribosome assembly is not known, the purification of pre-ribosomes using these assembly factors (e.g. Utp23 or Kri1) would at the same time provide the opportunity to learn more about their function and interaction with snR30. For example, it would be interesting to discover whether all or only a fraction of pre-ribosomes purified with Utp23 or Kri1 are also bound by snR30 [52]. Another possibility would be to tag core H/ACA proteins such as Cbf5/dyskerin for enrichment of snR30;

however, this strategy may also purify other pre-ribosome-snoRNA complexes due to the presence of the H/ACA core proteins across a wide array of RNPs beyond the pre-ribosome [48]. For the study of snR30, the direct tagging of snR30 is therefore the first choice method of ensuring the enrichment of snR30 bound particles while alternative strategies may be pursued later.

Based on the data presented here, I have effectively assembled this system and demonstrated over the course of multiple purifications that the system is capable of generating a homogenous population of complexes that contain both the rRNA precursor and snR30. Despite an inconsistent output of pre-ribosome amounts, I have further shown that the purification of pre-ribosomes can be accomplished with sufficient amounts and quality of the product for further analysis in at least one case, as further explained below.

The first goal of this project was the development of *S. cerevisiae* strains that can effectively serve as a source to purify pre-ribosomal particles. This goal required the introduction of sequences coding for RNA aptamers into RNA genes for specific affinity purifications. RNA aptamers are structural RNA elements that allow for the selective purification of specific RNAs using affinity chromatography [58, 60]. I accomplished this by generating a pRS313-derived plasmid containing tagged snR30, which was combined with existing pESC-Leu-based plasmids containing tagged truncations of rRNA. The two pESC-Leu-derived plasmids containing truncations of rRNA are induced by the presence of galactose and the absence of glucose via the action of a Gal promoter. While the transcription of the truncated pre-rRNA by PolII, as opposed to PolI, may be a concern, previous work of other labs has demonstrated that the ribosomal complexes produced by rRNA truncation are equivalent to cellular pre-ribosomes regardless of the polymerase used to transcribe the rRNA [40, 64]. The generation of the pRS313-snR30-5′Tob plasmid was accomplished by insertional mutagenesis within a pUC19-snR30 plasmid and ligation into a pRS313 backbone. These two plasmids, pRS313-snR30-

5′Tob and pESC-Leu-rRNA, can be co-transformed into the same strain of *S. cerevisiae* YDU1 allowing growth of the co-transformed strain in selective SC-His-Leu media. The growth of YDU1-5′Tob while exposed to doxycycline demonstrates that the 5′Tob variant of snR30 is functional as the presence of doxycycline represses the growth of YDU1 unless complemented with functional snR30. My earlier attempts to tag snR30 (data not shown) had shown that the tagging of snR30 in certain locations fails to complement the activity of the snR30-repressed strains. However, the choice to include the tobramycin aptamer within the 5′ hairpin, based both on published experiments tagging snR30 and the knowledge that the 5′ hairpin is functionally unimportant, proved more successful in producing strains of *S. cerevisiae* that are able to express both MS2-tagged rRNA truncations and tobramycin-tagged snR30 in an snR30-repressible background [28, 40, 42].

5.2 Optimization of the purification process

5.2.1 Measures of success

In order for the purification of snR30-associated pre-ribosomes to be useful in the analysis of the function and composition of the snR30 RNP in complex with the pre-ribosome, two criteria have to be met. These criteria are: (a) that a sufficient amount of the pre-ribosome is purified for analysis and (b) that the particle is purified to sufficient homogeneity representing intact particles without the significant presence of contaminants and fragmented particles. With respect to purifying sufficient amounts (criterion a), the two most likely avenues for further analysis of these pre-ribosomal particles are mass spectrometry for the determination of protein content and cryo-electron microscopy to determine the structure of the purified complex. It is predicted, based on established literature, that cryo-EM of pre-ribosomal particles will require tens of microliters of a sample with an absorbance at 260 nm of approximately 2 [18, 25, 37]. This is achievable by the concentration via centrifugal concentrators of a sample with a total A_{260} of at least 0.2 in a 1.5 mL elution from the tobramycin affinity purification [31, 37]. Due to the ability to concentrate samples without concern for denaturing of the ribosomal components,

mass spectrometry may be attempted for samples of a lower total A_{260} [28]. Concentration of samples for mass spectrometry can therefore be accomplished through methods such as trichloroacetic acid precipitation. Based on communications from the mass spectrometry facility at the University of Manitoba, roughly 25 μg of protein is required. With 1.5 mL elutions, this value corresponds theoretically to an elution A_{280} value of 0.025. However, this method still requires a minimum concentration to be feasible, as indicated by failures to effectively concentrate the elution fractions of purification 6. The amount of protein in this sample, as indicated by an A_{280} value of 0.0301, was not able to be concentrated effectively by precipitation. This indicates that a larger amount of pre-ribosomes within an elution will be required for mass spectrometry, especially to achieve the technical replicates that are standard for this analysis [28, 40].

For the second criterion, the homogeneity of a particle can be indirectly inferred from the behaviour of the tagged RNAs within the chromatography steps of the purification. For a successful purification via affinity chromatography, it is expected that the target molecule will be present in the elution from the resin but not in the late washes. This pattern of enrichment demonstrates that the complex is bound to a column stably, which allows for the removal of other biomolecules in the washes. The presence of both target RNAs across both the maltose affinity and tobramycin affinity purifications indicates that the two RNAs are associated, presumably as part of an intact particle. Homogeneity can be directly confirmed by negative stain electron microscopy, which allows for the direct visualization of pre-ribosomal particles and judgment of the comparative size and shape of individual particles [31].

Overall, the most successful purification by far, in terms of product amount, was purification 5 (Figure 7). With a total A_{260} value of 0.2605 and A_{280} of 0.2146, this sample showed sufficient product for multiple runs of mass spectrometry and cryo-EM utilizing concentration factors as low as 10x. No other purification was able to replicate this success, with amounts recovered

being at most 1/5th of this value. Due to the consequences of freeze-thaw cycles, electron microscopy and mass spectrometry could not be performed on purification 5. While no purification achieved high values in the tobramycin affinity purification elution, purification 11 shows a total A_{260} value of 0.1621 in its maltose affinity purification elution (Figure 7 A). This indicates that if the tobramycin affinity purification had recovered more than 60% of the material, a final total absorbance of 0.1 could have been achieved, which would be sufficient for further analysis. Based on purification 5, which recovered more than 60% of the total absorbance at 260 nm of the maltose elution in its tobramycin elution, this is achievable (Figure 7). These observations together indicate that the final attempted purification, purification 11, was successful in its maltose purification step but not its tobramycin purification step.

While the homogeneity of purification 5 could not be assessed through negative stain-EM, the RT-PCR analysis shows the expected patterns for a successful purification, with the detection of tagged RNA in the final elution but not the late washes. This indicates that it is at least likely that this pre-ribosome preparation was effectively purified to the point of homogeneity. Purification 6, despite having a lower yield, was analyzed by negative stain-EM, and only particles of a consistent and expected size were seen (Figure 9). While later purifications were not analyzed by electron microscopy, the RT-PCR analysis shows a consistent enrichment of RNA in the final elution for purification 5 and all following purifications. This indicates that despite the low amounts of product in the majority of purifications, the later purifications saw effective purification of homogenous populations.

5.2.2 Optimization of expression conditions

The optimization of the expression conditions is a necessary step in achieving effective purification of the target complexes. The amount of ribosomes produced by a cell is highly varied and regulated not just through the transcription of the rRNA but through the production and availability of the r-proteins and assembly factors and varies throughout the cell cycle [15,

65]. As well it was also necessary to fine-tune the number of cells that would be harvested for each purification, with consideration given to both the desired amount of product and the practical limits of growing large volumes of culture. In earlier purifications, such as purification 2, the cells are grown into stationary phase, and the target complex is not detectable in the RT-PCR analysis (Figure 2). However, by adjusting the growth conditions to harvest cells after ~2 doubling times and well before stationary phase (OD_{600} <1.1), I was able to achieve a larger amount of pre-ribosomal particles in the later purifications as would be expected from cells that must produce ribosomes to allow for rapid growth. Due to the lower number of cells in a culture at an OD_{600} of 1.1 than in a culture grown into stationary phase, it was necessary to increase the scale of the expression concurrently with this change to ensure that the number of cells was sufficient for the purification to yield detectable and analyzable amounts of pre-ribosomes. With the combination of these two changes, the experimental system begins to yield consistently detectable complexes and improved amounts of pre-ribosomes (Figure 3).

Further changes to the expression conditions of note are seen in purification 10, where I introduced an increased concentration of doxycycline to ensure the full repression of wild type snR30 within the cells. The tetracycline/doxycycline titratable promoter used in these cells responds in a dose-dependent manner to the presence of doxycycline [66]. The increased dosage of doxycycline does not increase the amount of purified ribosomes to levels seen in the highest yield purification, although it is possible that it contributed to the larger amount of product seen in purification 11 relative to the purifications immediately prior (Figure 11). Purifications 10 and 11 also saw the growth of cells in non-selective YPG medium. This functions to provide a richer growth medium for cells as opposed to the selective SC-His-Leu medium. There appears to be no effect of the media change on the amount of pre-ribosome yield from the associated purifications (Figure 10, 11).

5.2.3 Optimizations of stability

Throughout the iterative optimization process of the purifications, the precipitation of proteins during the binding of the samples to the tobramycin resin occurred on multiple occasions (Figure 2 G, Appendix). The resolution of this problem is dependent on the relative stability of the pre-ribosome complex and its constituents within the buffer system of the purification. The first improvement to overcome this problem was the adjustment of the buffer system used for the tobramycin purification. The initial buffer system (Table 3) was based on published purifications of pre-spliceosomes via a tobramycin-binding aptamer [62]. This buffer contained a lower concentration of HEPES than the maltose affinity purification buffers (20 mM vs 100 mM) as well as a lower concentration of salt (150 mM NaCl vs 200 mM KCl). Beginning with purification 5, the tobramycin buffer was adjusted to contain 100 mM HEPES and 200 mM KCl rather than 150mM NaCl such that it matches the maltose affinity purification buffers. In addition to reducing precipitation events, this change resulted in a dramatic improvement in the amount of product seen in purification 5, which is 10-fold higher than the previous purification (Figure 7). This indicates that the more concentrated HEPES buffer improved the stability of the pre-ribosome and the effectiveness of the purification. Additional improvements made to improve the stability of the complexes were increased washing of the tobramycin affinity resin following the blocking with ethanolamine and the consistent monitoring of pH at all steps of the purification. These improvements were attempted across the third and fourth purification and saw little to no improvement to the stability (Appendix Table A1).

Following purification 5, adjustments were made to further allow the future analysis of the purified particles. Samples of maltose affinity purification elution (Figure 3 F) were not suitable for mass spectrometry due to the presence of NP-40 detergent. In purification 6, the NP-40 detergent was removed from the resin via an extra washing with NP-40-free buffer prior to elution of the maltose affinity purification. This process resulted in further precipitation of the

proteins upon binding to the tobramycin affinity resin and was reverted prior to purification 10, which contained NP-40 again in the maltose affinity purification final washes elution. To further improve the stability of the pre-ribosomal complexes, the glycerol content of the buffers was increased to 20% from 10% starting with purification 10. This change further improved the stability of complexes, as seen in the lack of precipitation events in the following purifications.

5.2.4 Improvements to product amount

Throughout the iterations of purification improvement, only one purification (purification 6) saw sufficient amounts of pre-ribosomes for the attempt at negative stain-EM to be feasible (Figure 3). Negative stain-EM serves as a quality control step to determine the suitability of samples for cryo-EM and provides insight into sample homogeneity. The negative stain of purification 5 (data not shown) was unable to detect intact particles of an appropriate size to be pre-ribosomes. This was attributed to the destructive effects of sample storage at −80 °C and subsequent thawing.

Purification 6 was an attempt to replicate purification 5 with slight alterations to the buffer. The attempted replication in purification 6 proved unsuccessful in purifying the same amount of pre-ribosomes (Figure 8). The particles purified in purification 6 were able to be visualized by negative stain-EM (Figure 9). The size of the particles is consistent with the expected size of late pre-ribosomes, with the allowance of the detected particles being slightly smaller than the 90S particle visualized in Hunziker *et al.* 2019 [31] due to a lack of the proteins associated with the later stages of 18S rRNA transcription. The particles are also visibly isolated from notable amounts of smaller or differently shaped particles indicating homogeneity. The appearance of a proportion of the particles as dimers is a concern, however. The pre-ribosome is not expected to dimerize, and the presence of these particles could indicate that the particles have begun to aggregate even at low concentrations. It is also possible that the incomplete ribosome is prone to dimerization by a mechanism similar to the mechanism that drives dimerization of the mature

ribosome in prokaryotes during cellular stress [67]. In either case the further analysis of the pre-ribosomes, including a determination of how significant a portion of the pre-ribosomes are subject to this dimerization in not possible without an increase in the amount of ribosomes visualized on a singe grid. Further attempts to improve the product amount culminated with the increase of resin volume in purifications 10 and 11. The increases in resin volume were anticipated to provide a greater number of binding sites for both RNA aptamers, thereby increasing the number of pre-ribosomes associated with the resin. While this approach showed moderate improvements when used to purify particles from the YDU1-central-5′Tob strain (Figure 8), no iterations (including those with highly similar conditions) yielded more than 15% of the pre-ribosome amount detected in the tobramycin affinity resin elutions of purification 5 (Figure 3). The improvements of increasing resin volume are noticeable during the maltose affinity purification wherein the terminal purification, purification 11, shows similar amounts of product in the elution of this purification as the most successful purification, purification 6 (Figures 3, 7). These amounts are measured by the A_{260} values of 0.2835 in purification 5 compared to 0.1621 in purification 11. This observation leads to the conclusion that despite improvements overall to the pre-ribosome purifications, there is a high amount of variation in the yields of the tobramycin affinity purification that is not directly attributable to the protocol changes. Despite this, the amount of particles isolated, especially in the maltose affinity purification, has been improved. Taken together, the data characterizing the optimizations of the purification process indicate that I have improved the process of purifying snR30-associated pre-ribosomes. The process has been shown to produce detectable amounts of particles of a sufficient level of homogeneity for further analysis. The remaining steps of improving the amount of pre-ribosome particles recovered from the tobramycin affinity purification provide the only obstacle in producing sufficiently purified samples for analysis of the function of snR30.

5.3 Future directions

Throughout the course of optimizing my purification of the snR30-associated pre-ribosome, it has become clear that the amount of ribosomal particles in my final elution of the tobramycin affinity purification is highly varied. This issue has several potential causes, and the first step towards further optimizing this system is identifying and addressing the cause. A possible factor affecting the tobramycin resin is the repeated freeze-thaw cycles that the uncoupled resin (affigel-10) is subjected to with each separate resin preparation. While the uncoupled resin is stable at −80 °C, it has been subjected to multiple freeze-thaw cycles between purifications 5 and 11. It is possible that these cycles damaged the resin and reduced its binding capacity. Furthermore, it is also possible that the separate preparation of tobramycin-coupled Affigel for each purification introduces variance due to the minor differences in sample preparation, such as ambient temperature changes and handling time between transfer to the centrifuges and/or nutator. To address these issues, I will perform further test purifications with a new batch of affigel-10 resin, prepared either individually or in large batches. In parallel, other members of our lab will undertake experiments testing the binding of an *in vitro* prepared 5′Tob-snR30 RNA to examine the capacity changes of the affigel-10 resin in a manner that is more easily quantified than the purification of snR30 from a mixed cellular lysate.

Furthermore, I will make attempts to further stabilize the interaction of snR30 to the pre-ribosomes via alteration of the expression conditions. Unlike all other H/ACA snoRNAs, snR30 requires the activity of a helicase, Rok1, for release. If Rok1 was depleted during the expression of the pre-ribosomes, it is likely that a higher proportion of pre-ribosomes would be bound more stably to snR30. This change could potentially improve the amount of product seen across the tobramycin affinity purification. This strategy will have to take the essential nature of Rok1 into account as a knockout of the gene coding for Rok1 is not a viable method of achieving this goal. Instead a new yeast strain might be created on the YDU1 strain to include a decreased

abundance by mRNA perturbation (DAmP) tag on the ROK1 gene which disrupts the 3' untranslated region with a kanamycin resistance cassette that causes destabilization of the transcript [68]. However, this approach is not directly feasible since the YDU1 strain already contains a kanamycin resistance cassette which would have to be removed prior to insertion of the DAmP tag. The inclusion of this tag would result in a reduced abundance of the Rok1 protein due to the mRNA degradation caused by the DAmP tag. It has been shown that the inclusion of a DAmP tag is an effective way of reducing the abundance of essential proteins without abolishing cell growth [68]. The resulting strain could be utilized for the expression and subsequent purification of the dual aptamer tagged expression and purification system for snR30 bound pre-ribosomes described here. The inclusions of the DAmP tag in the ROK1 gene would alter the system such that the release of snR30 from the pre-ribosome would be impaired, but not to such an extent as to be lethal to the cell.

A depletion of Rok1 would also allow for alternative purification methods for the enrichment of the pre-ribosome. In this thesis I utilized the expression of truncated forms of the pre-rRNA to create an accumulation of a specific stage of ribosome assembly. The accumulation of a specific stage of the pre-ribosome is important for the purification as it avoids the problem posed by the fact that snR30 containing pre-ribosomes represent a small fraction of the pre-ribosomes in the cell. With the depletion of Rok1 and the accompanying reduction of snR30 release, the pre-ribosomes containing snR30 are predicted to become a larger portion of the ribosome precursors in a given cell. This would bypass the need for plasmid derived expression of rRNA truncations via the Gal promoter. Pre-ribosomes containing rRNA transcribed from genomic rDNA would be advantageous to purify as they would be complexes formed by the transcription of rRNA by PolI. While the transcription of rRNA by PolII has been shown to result in functional ribosomes, the process does not include the formation of a nucleolus [64]. Combining the depletion of Rok1 with the purification of pre-ribosomes via protein affinity chromatography

would allow for a comparison of PolI and PolII derived pre-ribosomes as well as providing an alternative method of enriching pre-ribosomes for later study of the snR30 bound fraction following enrichment of tobramycin-tagged snR30. In a Rok1 depleted system lacking the expression of MS2-tagged rRNA truncations, a further inclusion of a protein tag for affinity purification would need to be made to allow for the initial enrichment of SSU precursors. In previous studies, this has been accomplished using the tagging of Utp10 with green fluorescent protein via a cleavable linker and subsequent purification of complexes with green fluorescent protein antibody coated resin [40]. As an alternative, both Utp9 and Noc4 have been tagged with TAP tags to allow for the purification of pre-ribosomes [28]. In any of these cases, the purification of the pre-ribosome using the affinity of the protein tags for the appropriate resin would be followed by the usage of tobramycin-coupled resin to enrich for tobramycin-tagged snR30. This would represent an alterative strategy for the enrichment of the pre-ribosome. The study of complexes purified via this method could be used to complement the study of particles resulting from the enrichment by the expression of MS2-tagged rRNA truncations.

Finally, I will assess the success of the coupling of HMM and tobramycin to the dextrin sepharose and Affigel-10 resins, respectively. Standardizing and evaluating the resin preparation has the potential to reduce the variability of the preparations. The simplest method for the evaluation of the preparation of a resin is the quantification of the ligand before and after the coupling. In the case of HMM, quantification of the protein content that is binding by absorbance at 280 nm would allow for a determination of how much protein had bound to the column. Comparisons of the protein content of the initial solution to the content within the buffer washed from the column after would allow for quantification of the amount of protein bound. Given the high affinity of the HMM protein for the resin, I expect more than 50% of the protein to bind to the resin resulting in a significant reduction in absorbance after binding to the resin.

In the case of the preparation of the tobramycin affinity resin, a similar process could be performed by quantifying the amounts of tobramycin in the coupling buffer before and after the incubation with Affigel-10 resin. While this is rendered more difficult by the lack of absorbance of tobramycin, it is possible to employ a biosensor to quantify tobramycin in a sample in a quantitative manner [69]. However, this approach is further complicated by the fact that 100 mM tobramycin is used for coupling and that likely only a small fraction of tobramycin will covalently be linked to the resin resulting in a very small signal. Additionally, the binding capacity of the tobramycin-coupled resin can be measured. By performing *in vitro* transcription of RNAs containing either an MS2 aptamer or a tobramycin aptamer, a sample of pure RNA can be obtained. Since a sample of *in vitro* transcribed RNA could be easily quantified by spectrophotometry, the amount of tagged RNA that binds to a resin could be determined by the measurement of the RNA concentration of the eluted fraction from the resin. The measured yield of an RNA purification would serve as a benchmark for the successful coupling of a resin. Following the success of these improvements, the purification system for snR30-bound pre-ribosomes will then be exploited to begin answering the open questions surrounding snR30 as an assembly factor essential for the development of the small subunit ribosomal precursor.

5.4 Open questions surrounding snR30

The goal of this project has been to develop an experimental system to address questions surrounding the function of snR30 within the pre-ribosome. Despite being essential for the cleavages of the rRNA precursor at sites A_0, A_1, and A_2, snR30 is not associated with the ribosomal precursor during these cleavage events. Therefore, to fully understand the role of snR30, it is necessary to characterize the changes to the ribosomal precursor introduced by the binding of snR30 during the transcription of the central domain of the 18S rRNA and how those changes continue to affect the pre-ribosome following the dissociation of snR30 during the transcription of the ITS1 region.

Perhaps the most effective method of answering these questions is the determination of high-resolution structures of the pre-ribosome across the timeline of snR30 association. This method has proven effective in understanding other processes within the ribosomal precursor, including the cleavage of A_1 and the removal of Nob1 in later stages of ribosome assembly [18, 21]. This structural analysis would allow for a determination of the contacts of snR30 to the pre-ribosome and the conformational changes to the rRNA that accompany snR30 binding. It would also allow for the direct mapping of the interactions of snR30 with its associated proteins and the changes to those interactions over the course of the ribosomal assembly process.

In particular, the release of snR30, which requires the presence of both Rok1 and Utp23, may prove to be an important quality control step for the correct alignment of other assembly factors, such as the nuclease Utp24. The combination of snR30 enrichment and selection for a specific stage of ribosome assembly would allow for the differentiation of particles near the end of the snR30 binding. Given ribosomal particles, including the 3′ minor domain, contain proportionally less snR30 than earlier particles, it is likely that this population contains a portion of ribosomes that have recently released snR30 [28]. Purification via maltose chromatography would, in that case, yield a population of pre-ribosomes that could be separated by tobramycin affinity into those particles immediately prior to and after the release of snR30. This analysis is of particular importance if snR30 is serving a regulatory role. The differences between these two structures would yield insight into how the rRNA folding changes following snR30 release, with the rRNA, potentially adopting its mature fold after snR30 release. The study of snR30 release could also show which, if any, assembly factors release concurrently with snR30.

Analysis of *S. cerevisiae* snR30 also has the potential to inform our understanding of the human homolog U17. While there are differences in the structure of U17 compared to snR30, its overall binding to the ribosome with the help of the m1 and m2 regions is conserved [42, 55]. Given recent advances in the separation of subcellular compartments in human cells [17], the dual

RNA aptamer system described here could be adapted for expression in human cells. This analysis, combined with new advances in the purification of ribosome precursors from human cells, would allow for the extraction of the human pre-ribosome bound to U17 [17]. The study of these complexes would be advantageous to answer several questions in regard to proteins whose function differs between yeast and humans, such as Utp23. The human homolog of the snR30-bound protein Utp23 is hUtp23. This protein is of interest in yeast due to its previously mentioned interactions with Utp24 but additionally in humans for its essential nuclease activity [55]. While Utp23 does not exhibit nuclease activity, hUtp23 does [55]. Analysis of U17 would also be greatly aided by assays that have been performed on snR30. *In vitro* binding assays measuring the affinity of U17 for hUtp23 would help to show to what extent the interaction of hUtp23 and U17 in humans is directly comparable to the interaction of Utp23 to snR30 in yeast. This is expected to be a tight binding if the system is homologous with snR30, as experiments have demonstrated the *in vitro* binding of yeast snR30 to Utp23 [52].

Both in humans and yeast, there remain further unanswered questions regarding snR30 and U17. The complexes formed by snR30, when not bound to the ribosome, have been assayed by pull-down assays, but no further analysis on the diversity of composition of the free snR30 RNP has been made [43]. The localization of the free snR30 RNP is also a question of great interest. Recent advances in cryo-electron tomography and fluorescence microscopy together have shown that the process of ribosome assembly takes place along a “cable” that forms around the rDNA [14, 15]. Protein assembly factors are recruited from reservoirs on the periphery of this cable to the actively assembling ribosome precursor. It is of interest in the context of snR30/U17 activity to determine if this behaviour is consistent with an RNA assembly factor. This question could be assayed using a variation of the herein-described snR30-5′Tob variant that contains a fluorescent RNA aptamer such as the MANGO aptamer. These aptamers allow for the binding and fluorescent activation of a small molecule dye that would allow the tracking of snR30 *in vivo*

once this dye is introduced [70]. The introduction of the MANGO aptamer could further be used in Förster resonance energy transfer experiments to determine the real time proximity of snR30 another molecule containing an appropriate fluorescent tag such as another snoRNA, an rRNA expansion segment or an assembly factor.

5.6 Conclusion

In this thesis, I have presented the development and optimization of a system for the purification of the snR30-associated pre-ribosome from yeast. This system is an important step in fully understanding the function of snR30, both in terms of the interactions it makes within the pre-ribosome and how those interactions facilitate the cleavage of the spacer regions of the rRNA precursor. This analysis is important to our understanding of the assembly of ribosomes in yeast and the role of functional RNAs within this process. In addition to elucidating the role of snR30 within yeast, these studies will inform investigations of U17 in humans. A further understanding of an essential step of ribosome assembly makes it a potential therapeutic target for diseases of ribosome assembly. Particularly, each essential step of ribosome assembly becomes a potential target for therapeutics aimed at reducing the overproduction of ribosomes in cancer cells [4, 68]. It is also possible, given the complex interactions of factors within the pre-ribosomes, that analysis of snR30 may give insights into the nature of ribosomopathies stemming from the disruption of other linked assembly factors once the full interaction network of snR30 is better characterized.

References

1. Alcindor, T. and N. Beauger, *Oxaliplatin: a review in the era of molecularly targeted therapy.* Curr Oncol, 2011. **18**(1): p. 18-25.
2. Brighenti, E., D. Trere, and M. Derenzini, *Targeted cancer therapy with ribosome biogenesis inhibitors: a real possibility?* Oncotarget, 2015. **6**(36): p. 38617-27.
3. Nicolas, E., et al., *Involvement of human ribosomal proteins in nucleolar structure and p53-dependent nucleolar stress.* Nat Commun, 2016. **7**: p. 11390.
4. Penzo, M., et al., *The Ribosome Biogenesis-Cancer Connection.* Cells, 2019. **8**(1).
5. Angelini, M., et al., *Missense mutations associated with Diamond-Blackfan anemia affect the assembly of ribosomal protein S19 into the ribosome.* Hum Mol Genet, 2007. **16**(14): p. 1720-7.
6. Devlin, J.R., et al., *Combination Therapy Targeting Ribosome Biogenesis and mRNA Translation Synergistically Extends Survival in MYC-Driven Lymphoma.* Cancer Discov, 2016. **6**(1): p. 59-70.
7. Narla, A. and B.L. Ebert, *Ribosomopathies: human disorders of ribosome dysfunction.* Blood, 2010. **115**(16): p. 3196-205.
8. Babaian, A., et al., *Loss of m1acp3Ψ Ribosomal RNA Modification Is a Major Feature of Cancer.* Cell Reports, 2020. **31**(5): p. 107611.
9. Bustelo, X.R. and M. Dosil, *Ribosome biogenesis and cancer: basic and translational challenges.* Curr Opin Genet Dev, 2018. **48**: p. 22-29.
10. Klinge, S. and J.L. Woolford, Jr., *Ribosome assembly coming into focus.* Nat Rev Mol Cell Biol, 2019. **20**(2): p. 116-131.
11. Thomson, E., S. Ferreira-Cerca, and E. Hurt, *Eukaryotic ribosome biogenesis at a glance.* J Cell Sci, 2013. **126**(Pt 21): p. 4815-21.
12. Sloan, K.E., et al., *Tuning the ribosome: The influence of rRNA modification on eukaryotic ribosome biogenesis and function.* RNA Biol, 2017. **14**(9): p. 1138-1152.
13. Barandun, J., et al., *The complete structure of the small-subunit processome.* Nat Struct Mol Biol, 2017. **24**(11): p. 944-953.
14. Lin, S., et al., *Production of nascent ribosome precursors within the nucleolar microenvironment of Saccharomyces cerevisiae.* Genetics, 2022. **221**(3).
15. Tartakoff, A.M., et al., *The nucleolus as a polarized coaxial cable in which the rDNA axis is surrounded by dynamic subunit-specific phases.* Curr Biol, 2021. **31**(12): p. 2507-2519 e4.
16. Erdmann, P.S., et al., *In situ cryo-electron tomography reveals gradient organization of ribosome biogenesis in intact nucleoli.* Nat Commun, 2021. **12**(1): p. 5364.
17. Nieto, B., et al., *Efficient fractionation and analysis of ribosome assembly intermediates in human cells.* RNA Biol, 2021. **18**(sup1): p. 182-197.
18. Cheng, J., et al., *90S pre-ribosome transformation into the primordial 40S subunit.* Science, 2020. **369**(6510): p. 1470-1476.
19. Vanrobays, E., et al., *Processing of 20S pre-rRNA to 18S ribosomal RNA in yeast requires Rrp10p, an essential non-ribosomal cytoplasmic protein.* EMBO J, 2001. **20**(15): p. 4204-13.
20. Huang, H., M. Parker, and K. Karbstein, *The modifying enzyme Tsr3 establishes the hierarchy of Rio kinase binding in 40S ribosome assembly.* RNA, 2022. **28**(4): p. 568-582.

21. Mitterer, V., et al., *Conformational proofreading of distant 40S ribosomal subunit maturation events by a long-range communication mechanism.* Nat Commun, 2019. **10**(1): p. 2754.
22. Kos, M. and D. Tollervey, *Yeast pre-rRNA processing and modification occur cotranscriptionally.* Mol Cell, 2010. **37**(6): p. 809-20.
23. Henras, A.K., E. Bertrand, and G. Chanfreau, *A cotranscriptional model for 3'-end processing of the Saccharomyces cerevisiae pre-ribosomal RNA precursor.* RNA, 2004. **10**(10): p. 1572-85.
24. Hadjiolova, K.V., et al., *Alternative pre-rRNA processing pathways in human cells and their alteration by cycloheximide inhibition of protein synthesis.* Eur J Biochem, 1993. **212**(1): p. 211-5.
25. Hunziker, M., et al., *UtpA and UtpB chaperone nascent pre-ribosomal RNA and U3 snoRNA to initiate eukaryotic ribosome assembly.* Nat Commun, 2016. **7**: p. 12090.
26. Lebaron, S., et al., *Rrp5 binding at multiple sites coordinates pre-rRNA processing and assembly.* Mol Cell, 2013. **52**(5): p. 707-19.
27. Kudla, G., et al., *Cross-linking, ligation, and sequencing of hybrids reveals RNA-RNA interactions in yeast.* Proc Natl Acad Sci U S A, 2011. **108**(24): p. 10010-5.
28. Zhang, L., et al., *Stepwise and dynamic assembly of the earliest precursors of small ribosomal subunits in yeast.* Genes Dev, 2016. **30**(6): p. 718-32.
29. Chaker-Margot, M., et al., *Architecture of the yeast small subunit processome.* Science, 2017. **355**(6321).
30. Martin, R., et al., *A pre-ribosomal RNA interaction network involving snoRNAs and the Rok1 helicase.* RNA, 2014. **20**(8): p. 1173-82.
31. Hunziker, M., et al., *Conformational switches control early maturation of the eukaryotic small ribosomal subunit.* eLife, 2019. **8**.
32. Wells, G.R., et al., *The PIN domain endonuclease Utp24 cleaves pre-ribosomal RNA at two coupled sites in yeast and humans.* Nucleic Acids Res, 2016. **44**(11): p. 5399-409.
33. Bohnsack, K.E., C. Hobartner, and M.T. Bohnsack, *Eukaryotic 5-methylcytosine (m(5)C) RNA Methyltransferases: Mechanisms, Cellular Functions, and Links to Disease.* Genes (Basel), 2019. **10**(2).
34. Caton, E.A., et al., *Efficient RNA pseudouridylation by eukaryotic H/ACA ribonucleoproteins requires high affinity binding and correct positioning of guide RNA.* Nucleic Acids Res, 2018. **46**(2): p. 905-916.
35. Kister, K.P., B. Muller, and W.A. Eckert, *Complex endonucleolytic cleavage pattern during early events in the processing of pre-rRNA in the lower eukaryote, Tetrahymena thermophila.* Nucleic Acids Res, 1983. **11**(11): p. 3487-502.
36. Parker, M.D., et al., *A kinase-dependent checkpoint prevents escape of immature ribosomes into the translating pool.* PLoS Biol, 2019. **17**(12): p. e3000329.
37. Du, Y., et al., *Cryo-EM structure of 90S small ribosomal subunit precursors in transition states.* Science, 2020. **369**(6510): p. 1477-1481.
38. Braun, C.M., et al., *Pol5 is required for recycling of small subunit biogenesis factors and for formation of the peptide exit tunnel of the large ribosomal subunit.* Nucleic Acids Res, 2020. **48**(1): p. 405-420.
39. Reichow, S.L., et al., *The structure and function of small nucleolar ribonucleoproteins.* Nucleic Acids Res, 2007. **35**(5): p. 1452-64.
40. Chaker-Margot, M., et al., *Stage-specific assembly events of the 6-MDa small-subunit processome initiate eukaryotic ribosome biogenesis.* Nat Struct Mol Biol, 2015. **22**(11): p. 920-3.
41. Morrissey, J.P. and D. Tollervey, *U14 small nucleolar RNA makes multiple contacts with the pre-ribosomal RNA.* Chromosoma, 1997. **105**(7-8): p. 515-22.

42. Atzorn, V., P. Fragapane, and T. Kiss, *U17/snR30 Is a Ubiquitous snoRNA with Two Conserved Sequence Motifs Essential for 18S rRNA Production.* Molecular and Cellular Biology, 2004. **24**(4): p. 1769-1778.
43. Lemay, V., et al., *Identification of novel proteins associated with yeast snR30 small nucleolar RNA.* Nucleic Acids Res, 2011. **39**(22): p. 9659-70.
44. Bohnsack, M.T., M. Kos, and D. Tollervey, *Quantitative analysis of snoRNA association with pre-ribosomes and release of snR30 by Rok1 helicase.* EMBO Rep, 2008. **9**(12): p. 1230-6.
45. Barandun, J., M. Hunziker, and S. Klinge, *Assembly and structure of the SSU processome - a nucleolar precursor of the small ribosomal subunit.* Current Opinion in Structural Biology, 2018. **49**: p. 85-93.
46. Kiss, T., *Small nucleolar RNA-guided post-transcriptional modification of cellular RNAs.* EMBO J, 2001. **20**(14): p. 3617-22.
47. Fayet-Lebaron, E., et al., *18S rRNA processing requires base pairings of snR30 H/ACA snoRNA to eukaryote-specific 18S sequences.* EMBO J, 2009. **28**(9): p. 1260-70.
48. Vos, T.J. and U. Kothe, *snR30/U17 Small Nucleolar Ribonucleoprotein: A Critical Player during Ribosome Biogenesis.* Cells, 2020. **9**(10).
49. Liu, J.M. and S.R. Ellis, *Ribosomes and marrow failure: coincidental association or molecular paradigm?* Blood, 2006. **107**(12): p. 4583-8.
50. Sy, B., et al., *High-Resolution, High-Throughput Analysis of Hfq-Binding Sites Using UV Crosslinking and Analysis of cDNA (CRAC).* Bacterial Regulatory Rna: Methods and Protocols, 2018. **1737**: p. 251-272.
51. McCaughan, U.M., et al., *Pre-40S ribosome biogenesis factor Tsr1 is an inactive structural mimic of translational GTPases.* Nat Commun, 2016. **7**: p. 11789.
52. Vos, T.J. and U. Kothe, *Synergistic interaction network between the snR30 RNP, Utp23, and ribosomal RNA during ribosome synthesis.* RNA Biol, 2022. **19**(1): p. 764-773.
53. Cheng, J., et al., *3.2-A-resolution structure of the 90S preribosome before A1 pre-rRNA cleavage.* Nat Struct Mol Biol, 2017. **24**(11): p. 954-964.
54. Hoareau-Aveilla, C., et al., *Utp23p is required for dissociation of snR30 small nucleolar RNP from preribosomal particles.* Nucleic acids research, 2012. **40**(8): p. 3641-3652.
55. Wells, G.R., et al., *The ribosome biogenesis factor yUtp23/hUTP23 coordinates key interactions in the yeast and human pre-40S particle and hUTP23 contains an essential PIN domain.* Nucleic Acids Res, 2017. **45**(8): p. 4796-4809.
56. Doherty, M.K., et al., *Turnover of the human proteome: determination of protein intracellular stability by dynamic SILAC.* J Proteome Res, 2009. **8**(1): p. 104-12.
57. Slobodin, B. and J.E. Gerst, *A novel mRNA affinity purification technique for the identification of interacting proteins and transcripts in ribonucleoprotein complexes.* RNA (New York, N.Y.), 2010. **16**(11): p. 2277-2290.
58. Yoon, J.H. and M. Gorospe, *Identification of mRNA-Interacting Factors by MS2-TRAP (MS2-Tagged RNA Affinity Purification).* Rna-Protein Complexes and Interactions: Methods and Protocols, 2016. **1421**: p. 15-22.
59. Batey, R.T. and J.S. Kieft, *Improved native affinity purification of RNA.* RNA, 2007. **13**(8): p. 1384-9.
60. Hartmuth, K., et al., *Protein composition of human prespliceosomes isolated by a tobramycin affinity-selection method.* Proc Natl Acad Sci U S A, 2002. **99**(26): p. 16719-24.
61. Leppek, K. and G. Stoecklin, *An optimized streptavidin-binding RNA aptamer for purification of ribonucleoprotein complexes identifies novel ARE-binding proteins.* Nucleic Acids Res, 2014. **42**(2): p. e13.
62. Hogg, J.R. and K. Collins, *RNA-based affinity purification reveals 7SK RNPs with distinct composition and regulation.* RNA, 2007. **13**(6): p. 868-80.

63. LaRonde-LeBlanc, N. and A. Wlodawer, *The RIO kinases: an atypical protein kinase family required for ribosome biogenesis and cell cycle progression.* Biochim Biophys Acta, 2005. **1754**(1-2): p. 14-24.
64. Nogi, Y., R. Yano, and M. Nomura, *Synthesis of large rRNAs by RNA polymerase II in mutants of Saccharomyces cerevisiae defective in RNA polymerase I.* Proc Natl Acad Sci U S A, 1991. **88**(9): p. 3962-6.
65. Lim, F. and D.S. Peabody, *Mutations that increase the affinity of a translational repressor for RNA.* Nucleic Acids Res, 1994. **22**(18): p. 3748-52.
66. Gari, E., et al., *A set of vectors with a tetracycline-regulatable promoter system for modulated gene expression in Saccharomyces cerevisiae.* YEAST, 1997. **13**(9): p. 837-848.
67. Akanuma, G., et al., *Ribosome dimerization is essential for the efficient regrowth of Bacillus subtilis.* Microbiology (Reading), 2016. **162**(3): p. 448-458.
68. Schuldiner, M., et al., *Exploration of the function and organization of the yeast early secretory pathway through an epistatic miniarray profile.* Cell, 2005. **123**(3): p. 507-19.
69. Cappi, G., et al., *Label-free detection of tobramycin in serum by transmission-localized surface plasmon resonance.* Anal Chem, 2015. **87**(10): p. 5278-85.
70. Autour, A., et al., *Fluorogenic RNA Mango aptamers for imaging small non-coding RNAs in mammalian cells.* Nat Commun, 2018. **9**(1): p. 656.

Appendix

Table A1: Supplemental table exhaustively listing purifications.

Purification	Strain	Media	Maltose Buffer	Tobramycin Buffer	Major Points of Failure
1	YDU1-Central-5′Tob	SC-His-Leu (2 L) +1.66 µg/mL	100mM HEPES pH 7.9 200mM KCl 1mM EDTA 1mM DTT 10mM βME 10% glycerol 0.02% NP-40	20mM HEPES pH 7.9 2mM MgCl2 150 mM NaCl 0.5 mM DTT 10% glycerol	Non-optimal storage conditions of cell pellet
2	YDU1-Central-5′Tob	SC-His-Leu (6 L) +1.66 µg/mL	100mM HEPES pH 7.9 200mM KCl 1mM EDTA 1mM DTT 10mM βME 10% glycerol 0.02% NP-40	20mM HEPES pH 7.9 2mM MgCl2 150 mM NaCl 0.5 mM DTT 10% glycerol	Precipitation during binding to tobramycin-Affigel
3	YDU1-Central-5′Tob	SC-His-Leu (6 L) +1.66 µg/mL	100mM HEPES pH 7.9 200mM KCl 1mM EDTA 1mM DTT 10mM βME 10% glycerol 0.02% NP-40	20mM HEPES pH 7.9 2mM MgCl2 150 mM NaCl 0.5 mM DTT 10% glycerol	
4	YDU1-Central-5′Tob	SC-His-Leu (6 L) +1.66 µg/mL	100mM HEPES pH 7.9 200mM KCl 1mM EDTA 1mM DTT 10mM βME 10% glycerol 0.02% NP-40	20mM HEPES pH 7.9 2mM MgCl2 150 mM NaCl 0.5 mM DTT 10% glycerol	
5	YDU1-Central-5′Tob	SC-His-Leu (6 L) +1.66 µg/mL	100mM HEPES pH 7.9 200mM KCl 1mM EDTA 1mM DTT 10mM βME 10% glycerol 0.02% NP-40	100mM HEPES pH 7.9 200mM KCl 2mM MgCl2 1mM EDTA 1mM DTT 10mM βME 10% glycerol	Samples subjected to freeze-thaw before structural analysis
6	YDU1-Central-5′Tob	SC-His-Leu (6 L) +1.66 µg/mL	100mM HEPES pH 7.9 200mM KCl 1mM EDTA 1mM DTT 10mM βME 10% glycerol 0.02% NP-40*	100mM HEPES pH 7.9 200mM KCl 2mM MgCl2 1mM EDTA 1mM DTT 10mM βME 10% glycerol	

Table A1 continued

Purification	Strain	Media	Maltose Buffer	Tobramycin Buffer	Major Points of Failure
7	YDU1-Central-5′Tob	SC-His-Leu (6 L) +1.66 µg/mL	100mM HEPES pH 7.9 200mM KCl 2mM MgCl2 1mM EDTA 1mM DTT 10mM βME 10% glycerol 0.02% NP-40*	100mM HEPES pH 7.9 200mM KCl 2mM MgCl2 1mM EDTA 1mM DTT 10mM βME 10% glycerol	Precipitation during binding to tobramycin-Affigel
8	YDU1-Central-5′Tob	SC-His-Leu (6 L) +1.66 µg/mL	100mM HEPES pH 7.9 200mM KCl 2mM MgCl2 1mM EDTA 1mM DTT 10mM βME 10% glycerol 0.02% NP-40*	100mM HEPES pH 7.9 200mM KCl 2mM MgCl2 1mM EDTA 1mM DTT 10mM βME 10% glycerol	
9	YDU1-Major-5′Tob	SC-His-Leu (6 L) +1.66 µg/mL	100mM HEPES pH 7.9 200mM KCl 2mM MgCl2 1mM EDTA 1mM DTT 10mM βME 10% glycerol 0.02% NP-40*	100mM HEPES pH 7.9 200mM KCl 2mM MgCl2 1mM EDTA 1mM DTT 10mM βME 10% glycerol	Precipitation during binding to tobramycin-Affigel
10	YDU1-Major-5′Tob	YPG (6 L) + 10 µg/mL	100mM HEPES pH 7.9 200mM KCl 2mM MgCl2 1mM EDTA 1mM DTT 10mM βME 20% glycerol 0.02% NP-40	100mM HEPES pH 7.9 200mM KCl 2mM MgCl2 1mM EDTA 1mM DTT 10mM βME 20% glycerol	
11	YDU1-Central-5′Tob	YPG (6 L) + 10 µg/mL	100mM HEPES pH 7.9 200mM KCl 2mM MgCl2 1mM EDTA 1mM DTT 10mM βME 20% glycerol 0.02% NP-40	100mM HEPES pH 7.9 200mM KCl 2mM MgCl2 1mM EDTA 1mM DTT 10mM βME 20% glycerol	